CO$_2$-Induced Sahel Greening in Three CMIP5 Earth System Models

Sebastian Bathiany

Max Planck Institute for Meteorology, Hamburg, Germany

Martin Claussen

*Max Planck Institute for Meteorology, and Centrum für Erdsystemforschung und Nachhaltigkeit,
Universität Hamburg, Hamburg, Germany*

Victor Brovkin

Max Planck Institute for Meteorology, Hamburg, Germany

(Manuscript received 29 August 2013, in final form 25 June 2014)

ABSTRACT

The existence and productivity of vegetation is the basis for food and energy supply in the Sahel. Past changes in climate and vegetation abundance have raised the question whether the region could become greener in the future as a result of higher CO$_2$ levels. By analyzing three Earth system models (ESMs) from phase 5 of the Coupled Model Intercomparison Project (CMIP5) with dynamic vegetation, the authors demonstrate why an answer to this question remains elusive in contrast to more robust projections of vegetation cover in the extratropics. First, it depends on the location and the time scale whether vegetation expands or retreats. Until the end of the twenty-first century, the three models agree on a substantial greening in the central and eastern Sahel due to increased CO$_2$ levels. This trend is reversed thereafter, and vegetation retreats in particular in the western Sahel because the beneficial effect of CO$_2$ fertilization is short lived compared to climate change. Second, the vegetation cover changes are driven by different processes in different models (most importantly, precipitation change and CO$_2$ fertilization). As these processes tend to oppose each other, the greening and browning trends are not a reliable result despite the apparent model agreement. The authors also find that the effect of vegetation dynamics on the surface energy balance crucially depends on the location. In contrast to the results of many previous studies, the Sahel appears as a hotspot where the physiological effects of CO$_2$ can exert a cooling because vegetation structure and distribution overcompensate for the decreased stomatal conductance.

1. Introduction

The Sahel is a climatic transition region where the supply of water, food, and even energy crucially depends on climate. Poverty, low development, and political conflicts tend to enforce this dependency and may even aggravate it in a future climate (Scheffran et al. 2012). The large population of the Sahel is therefore very vulnerable to climate variability (as the drought of the 1970s–80s demonstrated) and to anthropogenic climate change.

Reconstructions of vegetation abundance and climate show that northern Africa was much wetter and greener at the beginning of the mid-Holocene (Jolly et al. 1998a,b; Prentice et al. 2000; Lézine et al. 2011). In this period, the different Earth orbit enhanced the summer insolation in the Northern Hemisphere and thus the West African summer monsoon (Kutzbach 1981). Petit-Maire (1990) therefore posed the question "Will greenhouse green the Sahara?" and outlined a future between the two historical cases of an expanded desert during the last ice age and the green Sahara during the early Holocene. However, such analogies are of limited use for predictions, as the spatial pattern and the rate of change are very different for natural and anthropogenic forcing

(Petit-Maire 1990; Claussen et al. 2003). It is therefore unclear how natural vegetation in northern Africa will respond to the anthropogenic forcing scenarios of the next centuries. Trends in recent satellite observations are spatially inhomogeneous (de Jong et al. 2012), depend on the chosen time period (Anyamba and Tucker 2005; Fensholt and Rasmussen 2011), and are difficult to attribute (Fensholt and Rasmussen 2011).

Presumably, the most important drivers of future vegetation distribution in the Sahel are changes in land use, CO_2 concentration (because of its effect on vegetation physiology), and precipitation (caused by the radiative effect of CO_2). In this study, we only investigate the potential natural vegetation dynamics resulting from CO_2 concentration changes. These resulting changes in the vegetation composition and distribution are therefore not affected by any land-use change scenario but rather provide the precondition for future land use.

Changes in precipitation can occur for different reasons, which are difficult to separate in observations. First, a larger land–sea temperature contrast is expected to intensify the West African monsoon (WAM) (Monerie et al. 2012; Skinner et al. 2012). However, the effect of the radiative forcing of CO_2 over land on surface evaporation (Giannini 2010), atmospheric stability, and the distribution of moisture (Chou and Neelin 2004; Chou et al. 2009) must also be considered. Second, aerosols have been found to affect the monsoon system in model simulations (Ackerley et al. 2011; Kim et al. 2008). Third, there is evidence for an influence of SSTs in all major tropical and subtropical oceans (Giannini et al. 2003; Lu and Delworth 2005; Herceg et al. 2007; Cook 2008; Mohino et al. 2011; Patricola and Cook 2010). For example, in the Atlantic, an enhanced interhemispheric SST gradient with warmer water in the North Atlantic is believed to induce a northward shift of the intertropical convergence zone (ITCZ), which then affects Sahelian rainfall (Hoerling et al. 2006; Cook 2008), presumably as a result of an intensified West African westerly jet (WAWJ) (Pu and Dickinson 2012). There is evidence that, in the twentieth century, changes in SSTs have been the dominating driver of the observed decadal variability in Sahelian rainfall (Joly et al. 2007; Biasutti et al. 2008). Vegetation dynamics have probably enhanced this decadal component (Zeng et al. 1999). However, the quantitative attribution to SSTs in different ocean basins and the superimposed global warming trend is unclear (Rodríguez-Fonseca et al. 2011). In the future, it is probable that changes in SSTs will be less important than in the twentieth century, because the radiative forcing over land increases (Patricola and Cook 2010, 2011; Monerie et al. 2012) and may even become the dominant driver of Sahelian

rainfall changes (Haarsma et al. 2005; Biasutti et al. 2008; Giannini 2010).

For the productivity of vegetation, other aspects of the terrestrial moisture balance must also be considered. In particular, changes in evapotranspiration may offset precipitation trends. Furthermore, other environmental conditions will affect productivity and vegetation composition. In this regard, physiological effects of CO_2 become important, and these effects differ between the two relevant photosynthetic pathways: C3 and C4. First, higher levels of CO_2 tend to enhance the carboxylation efficiency of Rubisco in C3 plants. Second, elevated atmospheric CO_2 levels have been observed to decrease stomatal conductance (Field et al. 1995; Long et al. 2004; Ainsworth and Long 2005; Ainsworth and Rogers 2007; Leakey et al. 2009; Norby and Zak 2011). Therefore, they can result in decreased transpiration and increased soil moisture. This increased water-use efficiency can further enhance productivity in C3 as well as C4 plants (Long et al. 2004; Ainsworth and Rogers 2007; Leakey et al. 2009). The sum of both mechanisms is known as CO_2 fertilization. Consequently, the potential increase in net primary productivity (NPP) may allow an expansion of vegetation in arid regions (Mahowald 2007; Donohue et al. 2013). As we focus on land cover changes, we only refer to CO_2 fertilization because of its impact on vegetation distribution.

In contrast, we more generally refer to "physiological effects" to address any climatic changes arising from stomatal closure, not restricted to that caused by CO_2 fertilization. Model results show that the reduced transpiration and reduced low-level cloud cover due to CO_2-induced stomatal closure tend to warm the surface, especially over tropical forests (Doutriaux-Boucher et al. 2009; Andrews et al. 2011). This "physiological forcing" has been found to contribute more than 10% to the CO_2-induced warming over land (Sellers et al. 1996; Cox et al. 1999; Boucher et al. 2009; O'ishi et al. 2009; Cao et al. 2010). The physiological forcing generally refers to changes in stomatal closure assuming a fixed leaf area. However, increases in leaf area index (LAI) may occur as a result of the increased productivity and an altered vegetation distribution and composition. These changes can enhance precipitation because of the low albedo of vegetation (Otterman 1974; Charney 1975; Charney et al. 1975; Claussen 1997) and organic soils (Claussen 2009; Vamborg et al. 2011). Also, the expansion of vegetation into desert areas tends to increase evapotranspiration (Charney et al. 1977; Claussen 1997). It has been argued that such structural changes (LAI and vegetation distribution) could overcompensate for the effect of stomatal conductance change (Betts et al. 1997; Leipprand and Gerten 2006). Among other important environmental conditions besides CO_2 are temperature and nutrient

TABLE 1. Summary of the CMIP5 models analyzed in this study.

Modeling center	Institute ID	Model name	Expansion
Max Planck Institute for Meteorology	MPI-M	MPI-ESM-LR	Max Planck Institute Earth System Model, low resolution
Japan Agency for Marine-Earth Science and Technology, Atmosphere and Ocean Research Institute (The University of Tokyo), and National Institute for Environmental Studies	MIROC	MIROC-ESM	Model for Interdisciplinary Research on Climate (MIROC), Earth System Model
Met Office Hadley Centre	MOHC	HadGEM2-ES and HadGEM2-A	Hadley Centre Global Environment Model, version 2–Earth System and Hadley Centre Global Environment Model, version 2–Atmosphere only version of ES

availability, although changes in the latter are not considered in the simulations we analyze.

With regard to these interactions, it seems most appropriate to incorporate all substantial drivers of vegetation changes as well as the important interactions between vegetation and climate in order to assess the possible future vegetation distribution. In this study, we follow such an integrated view by analyzing results from three Earth system models (ESMs) from phase 5 of the Coupled Model Intercomparison Project (CMIP5) that include a dynamic vegetation model. However, it is not our intention to aim at a robust projection of Sahelian vegetation cover. In contrast, we address the main caveats that prevent a reliable projection, even if more models and simulations were available. These caveats involve the dependency of the different processes on location and the time horizon, as well as the large process and modeling uncertainty. As we will show, the three models provide a useful set in order to demonstrate these caveats.

2. Models and experiments

a. Models

In this study we analyze simulations performed by the ESMs MPI-ESM-LR (Giorgetta et al. 2013), HadGEM2-ES (Collins et al. 2011; Martin et al. 2011), and MIROC-ESM (Watanabe et al. 2011). These models (expansions and summaries for the CMIP5 models used in this study are provided in Table 1) include comprehensive descriptions of atmosphere and ocean circulation as well as terrestrial vegetation processes on time scales from minutes (stomatal conductance and photosynthesis) to centuries (changes in vegetation distribution). We do not analyze output from other CMIP5 models with dynamic vegetation

because either the experiments we analyze have not been performed with them or they were applied with prescribed vegetation cover fractions.

The Max Planck Institute for Meteorology (MPI) ESM in low resolution (MPI-ESM-LR) includes the general circulation models ECHAM6 (Stevens et al. 2013; Roeckner et al. 2003) for the atmosphere with a horizontal resolution of T63 (approximately 1.8°); the MPI Ocean Model (MPI-OM) (Jungclaus et al. 2013) for the ocean and sea ice (approximately 1.5°); and the Hamburg Model of the Ocean Carbon Cycle, version 5 (HAMOCC5) ocean biogeochemistry model (Ilyina et al. 2013; Maier-Reimer et al. 2005). Land–atmosphere exchange is represented by the Jena Scheme for Biosphere–Atmosphere Coupling in Hamburg (JSBACH) terrestrial vegetation model (Raddatz et al. 2007). Its photosynthesis schemes are based on Farquhar et al. (1980) for C3 plants and on Collatz et al. (1992) for C4 plants. In the experiments analyzed in this study, eight natural and four anthropogenic plant functional types (PFTs) are distinguished by JSBACH. A dynamic vegetation scheme (Brovkin et al. 2009) determines their cover fractions as well as the area fraction of total vegetation cover. The distribution of woody versus grass cover is determined by light competition and disturbances caused by fire and windthrow. Competition between different tree or grass types is based on the productivity of the individual types. Similarly, vegetation can establish wherever the environmental conditions allow a positive productivity (Reick et al. 2013). The preindustrial global vegetation distribution compares reasonably to the Vegetation Continuous Fields dataset (Hansen et al. 2007) derived from the Moderate Resolution Imaging Spectroradiometer (MODIS) (Fig. 1; see also Figs. 1 and 2 in Brovkin et al. 2013a). North Africa is covered by too much vegetation, especially in its western part. However, the LAI of this vegetation is small (less than 1) as a result of the dry
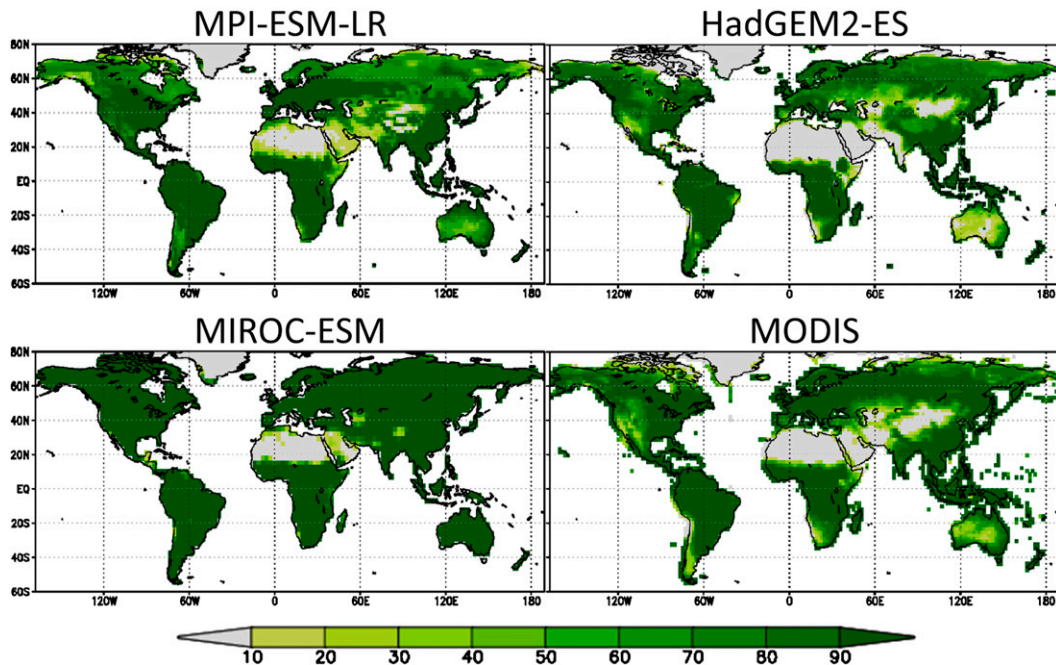
FIG. 1. Preindustrial distribution of vegetation in the three Earth system models (in % surface coverage) and present-day distribution in the VCF dataset from MODIS observations. The MODIS data have been converted to the resolution of MPI-ESM-LR. As the original data have a much higher resolution, small islands appear upscaled to the larger gridbox size.

climate. MPI-ESM-LR shows the strongest land carbon-concentration feedback (impact of CO_2 concentration on land uptake) of all CMIP5 ESMs compared in Arora et al. (2013). The direct effect of CO_2 on vegetation dynamics is therefore also expected to be large.

HadGEM2-ES comprises atmosphere, ocean and sea ice dynamics, terrestrial hydrology, and a terrestrial and marine carbon cycle. The horizontal resolution is approximately 1.25° latitude × 1.875° longitude. The interaction between land surface and atmosphere is calculated by the Met Office Surface Exchange Scheme, version 2 (MOSES2) (Essery et al. 2003). Leaf-level photosynthesis is based on Collatz's models for C3 (Collatz et al. 1991) and C4 plants (Collatz et al. 1992). Vegetation distribution and composition are calculated by the Top-Down Representation of Interactive Foliage and Flora Including Dynamics (TRIFFID) dynamic vegetation model (Cox 2001), which distinguishes five different plant types. Competition is based on NPP and height. The produced biomass is first used to increase the local carbon pools; in case of sufficient productivity, it is invested in the expansion of cover fractions. The deficiencies in the tropical vegetation distribution are too much forest cover as well as a too-southern Sahara–Sahel boundary (Fig. 1; see also Figs. 11 and 15 in Collins et al. 2011). HadGEM2-ES shows an above-average land carbon–concentration feedback when compared to other ESMs (Arora et al. 2013).

Like the other two models, MIROC-ESM includes general circulation models of atmosphere (resolution: T42; approximately 2.8°) and ocean. It also includes an ocean ecosystem model and the spatially explicit individual-based Dynamic Global Vegetation Model (SEIB-DGVM) terrestrial ecosystem model (Sato et al. 2007). SEIB calculates interactions between individual trees of a sample plot at each grid point. Its parameters have been tuned to match observations of forest structure and dynamics. A uniform grass layer is assumed to exist under the tree canopy. Vegetation is classified into 13 PFTs (11 trees and 2 grasses). Photosynthesis is calculated daily from temperature and the availability of light, CO_2, humidity, and soil moisture based on empirical relationships. Stomatal conductance is calculated following Ball et al. (1987) and Leuning (1995). Like MPI-ESM-LR and HadGEM2-ES, MIROC-ESM distinguishes different plant functional types, but, in contrast to the other two models, MIROC-ESM does not apply a tiling approach to describe the effect of vegetation dynamics. Instead, a representative patch with individual trees and an underlying grass cover is calculated and extrapolated to the gridbox size (Sato et al. 2007). The global distribution of trees partly depends on empirical relations with climate (e.g., because of establishment processes). A desert fraction is not directly defined within the model but classified as the area of natural vegetation

TABLE 2. Summary of the CMIP5 experiments analyzed in this study.

CMIP5 experiment	Expansion	Length	Forcings	Vegetation treatment	Number of realizations
RCP8.5	Representative concentration pathway 8.5	MPI-ESM-LR: 2006–2300 HadGEM2-ES: 2006–2299	prescribed CO_2 change and land-use change until 2100, no change in land use between 2100 and 2300	dynamic, except in areas of land use	MPI-ESM-LR: 1 HadGEM2-ES: 1 MIROC-ESM: 0
L2A8.5	XXXXX	MPI-ESM-LR and MIROC-ESM: 2006–2100 HadGEM2-ES: 2006–99	CO_2 change according to RCP8.5; land use fixed at year 2006 conditions	dynamic, except in areas of land use	MPI-ESM-LR: 2 HadGEM2-ES: 4 MIROC-ESM: 1
piControl	Preindustrial control	MPI-ESM-LR: 1000 yr HadGEM2-ES: 576 yr MIROC-ESM: 630 yr	no change in anthropogenic forcings	dynamic	All: 1
1pctCO2 (RADPHYS)	1 percent per year CO_2	140 yr	1% CO_2 increase per year, radiative and physiological effects active; no land-use change	dynamic	All: 1
esmFdbk1 (RAD)	ESM feedback 1	140 yr	1% CO_2 increase per year, radiative effect only; no land-use change	dynamic	All: 1
esmFixClim1 (PHYS)	ESM fixed climate 1	140 yr	1% CO_2 increase per year, physiological effect only; no land-use change	dynamic	All: 1
sstClim	Control SST climatology	30 yr	no change in anthropogenic forcings, SSTs and sea ice prescribed from piControl	vegetation distribution fixed, LAI interactive	MPI-ESM-LR: 1 HadGEM2-A: 1 MIROC-ESM: 0
sstClim4xCO2	SST climatology with $4 \times CO_2$ forcing	30 yr	as sstClim, but with instantaneously quadrupled CO_2	vegetation distribution fixed, LAI interactive	MPI-ESM-LR: 1 HadGEM2-A: 1 MIROC-ESM: 0

with an annual maximum LAI less than 0.2 (Sato et al. 2007) or with an annual NPP of 0 (T. Hajima 2013, personal communication). Although the CMIP5 vegetation cover fraction is therefore not exactly the same property as in the other two models, it is well comparable at the desert margins, where changes in the quantities of LAI, vegetation cover, and productivity are closely related. This is due to the common concept in all three models that an increased productivity drives the expansion of vegetation into a desert. Because of wet biases in MIROC-ESM, the global preindustrial distribution of deserts differs substantially from observations in the Northern Hemisphere, where no deserts other than the Sahara exist (Fig. 1). However, the position of the Sahara's southern margin is captured reasonably. MIROC-ESM has a comparatively small land carbon–concentration feedback (Hajima et al. 2012; Arora et al. 2013).

Since the models differ in the location and movement of the transition region between the Sahara and the tropical African forest, we do not show multimodel averages. Instead, we will follow a model-based definition of the Sahel as this transition region and define the desert boundary as the 80% vegetation cover line in each model.

b. Experiments

All simulations we analyze in this study (summaries and expansions of the CMIP5 experiments analyzed in this study are provided in Table 2) have been conducted within the latest Coupled Model Intercomparison Project and follow the setup described in Taylor et al. (2012). The models were forced by the radiative effects, biogeochemical effects, or the combination of both effects of increasing atmospheric CO_2 concentration. To this end, CO_2 concentrations are
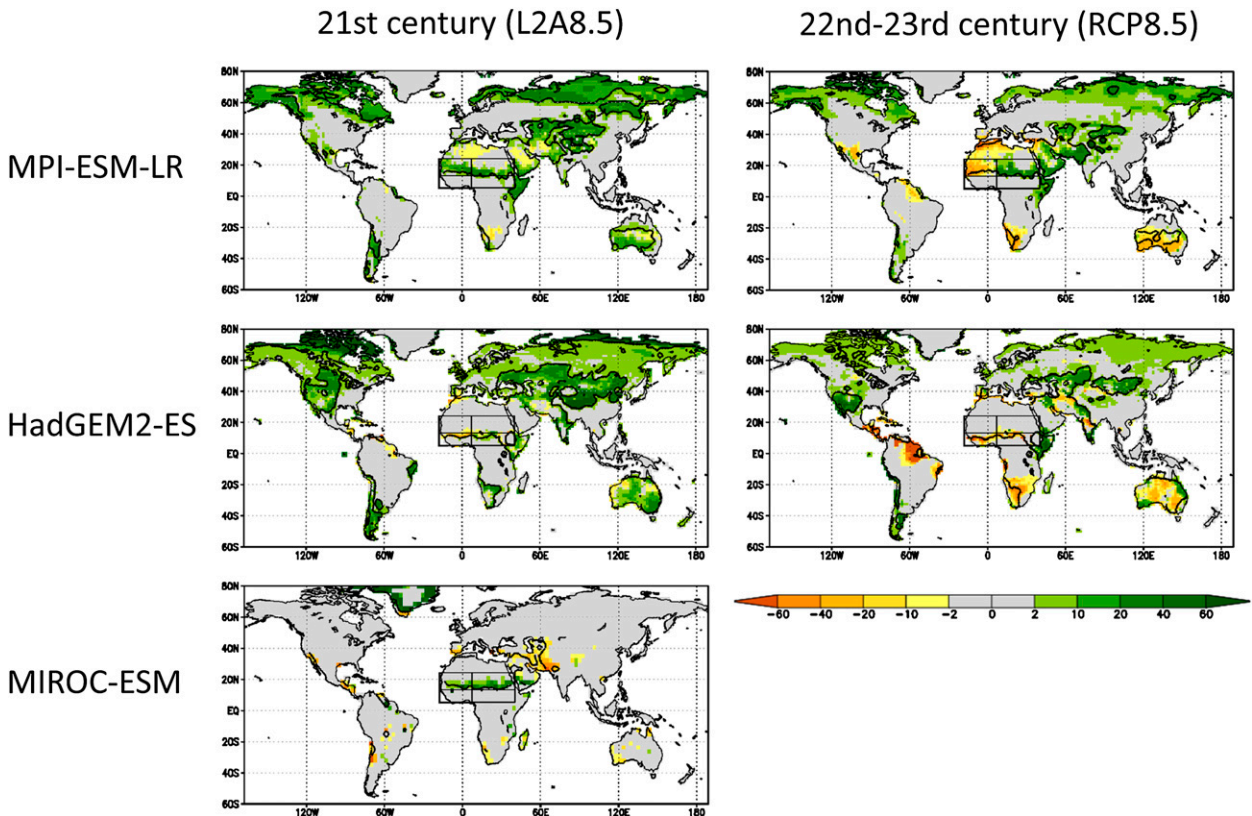
FIG. 2. Changes of vegetation cover (in %) in the RCP8.5 and L2A8.5 scenarios in three ESMs. The L2A8.5 maps show the difference between the last and first 10 yr of the experiment, averaged over all available realizations (Table 2). The RCP8.5 maps show the difference between averages over the last 10 yr and 2100–09. The black contours mark the boundary of 80% vegetation cover in the first 10 yr of each time period. Black rectangles mark the four areas referred to in Fig. 4 and in the text.

prescribed in all experiments and mostly follow an idealized trajectory.

In RCP8.5, the CO_2 concentration shows an accelerating increase until the year 2100 (when a radiative forcing of approximately $8.5 \, W \, m^{-2}$ is reached), followed by a stabilization period with a decelerating increase. In the year 2250, the CO_2 concentration reaches its final level of almost 2000 ppm. CO_2 concentration and radiative forcing both remain constant after the year 2250 (see Meinshausen et al. 2011, Figs. 4 and 5). In RCP8.5 we analyze the period 2100–2300 (extended RCP8.5) where the fractions of managed land were kept constant at year 2100 values. Before 2100, we analyze simulations with the identical CO_2 forcing where land use was fixed to the year 2006. These simulations are called L2A8.5 and were conducted within the Land-Use and Climate, Identification of Robust Impacts (LUCID) project (Pitman et al. 2009; Brovkin et al. 2013b). For MIROC-ESM, the extended RCP8.5 scenario was not available. Our combination of L2A8.5 and RCP8.5 and the fact that we do not analyze the differences between them allows us to exclude any

anthropogenic land-use changes (which occur in RCP8.5 before 2100).

In the idealized CMIP5 scenarios called 1pctCO2 (in the following: RADPHYS, to be consistent with similar studies before CMIP5), esmFdbk1 (RAD), and FixClim1 (PHYS), CO_2 is increased by 1% each year until CO_2 concentration has quadrupled after 140 years. In RAD, the CO_2 change only affects radiation, while the terrestrial vegetation sees preindustrial CO_2. In PHYS, the physiological effects of CO_2 are considered, but radiation is calculated from preindustrial CO_2. In RADPHYS, both effects of CO_2 are active. These experiments have been used to analyze feedbacks in the carbon cycle and their nonlinearity (Arora et al. 2013) but less so for the analysis of biogeophysical effects.

Finally, we analyze a preindustrial control simulation with climatological SSTs and sea ice (sstClim), and a similar simulation with quadrupled CO_2. In these experiments, both effects of CO_2, radiative and physiological, are active. However, because of the fixed ocean state, the forcings do not affect SSTs.
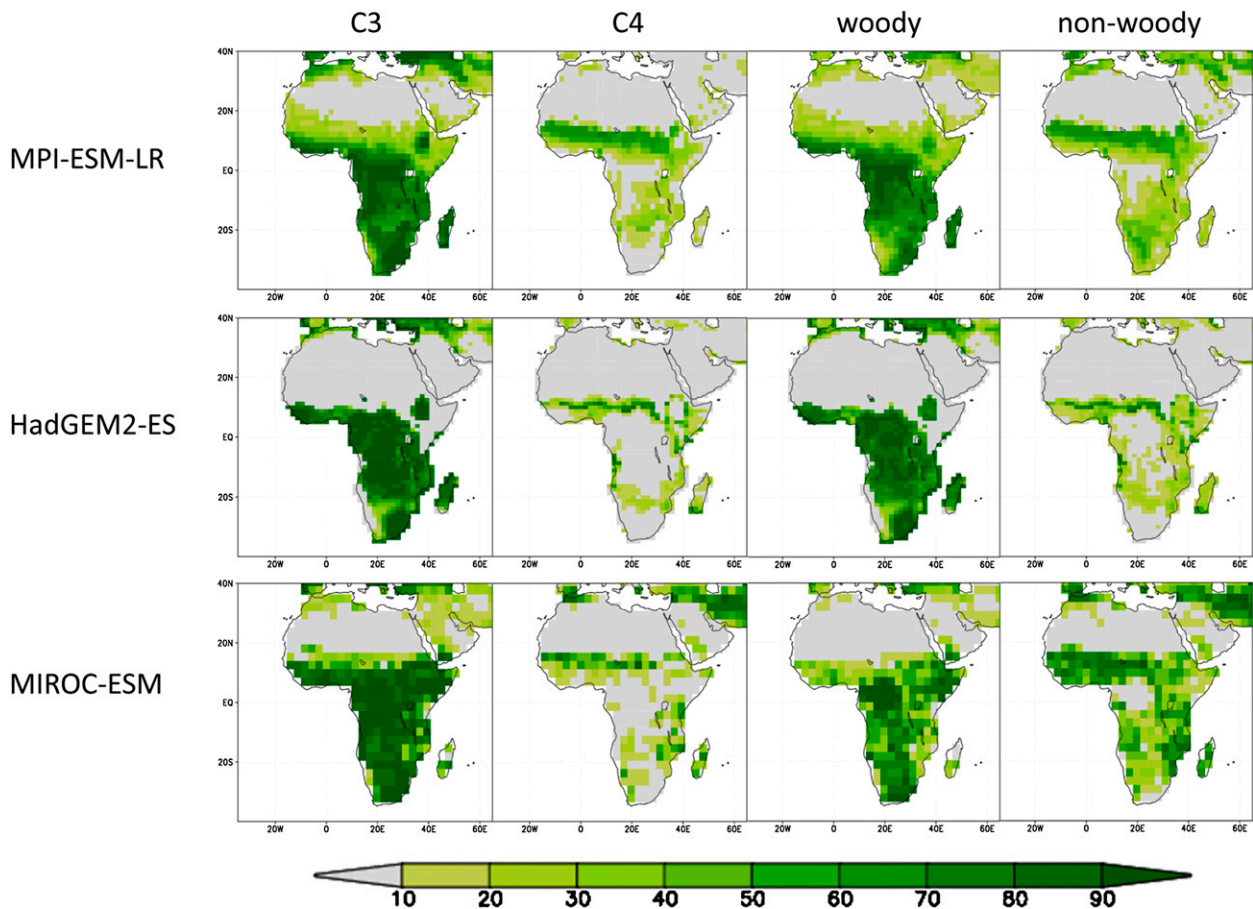
FIG. 3. Preindustrial composition of vegetation in terms of land cover fractions (in %) of C3 plants, C4 plants, woody plants (trees and shrubs), and nonwoody plants (natural grass, pasture and crops) in the three Earth system models.

3. Results

a. Comparison of vegetation cover changes

Figure 2 shows the changes of vegetation cover fraction for the three ESMs in response to the L2A8.5 and RCP8.5 concentration scenarios. In general, HadGEM2-ES and MPI-ESM-LR agree that there is a greening in the northern extratropics. In these areas, the increases in precipitation, warming, and CO_2 fertilization all tend to enhance the establishment of vegetation. Therefore, this extratropical greening agrees with expectations. MIROC-ESM shows no further greening in the extratropics (apart from outer Greenland) because the vegetation cover for present day is already 100% in these areas. As in the other two models, the LAI increases on most parts of the extratropical land.

Compared to the greening in the extratropics, vegetation changes are less robust and inhomogeneous in the tropics. However, MIROC-ESM and MPI-ESM-LR agree that there is a greening of the Sahel in response to increased atmospheric CO_2 levels until 2100. A greening

also occurs in parts of the central Sahel in HadGEM2-ES but not in the west. Interestingly, this zonal contrast also occurs in MPI-ESM-LR, but after 2100: In case of the very high CO_2 concentration in RCP8.5 toward the year 2300, the initial greening continues in the east but reverses in the western Sahel and Sahara. In contrast, HadGEM2-ES shows a southward expansion of the desert at all longitudes after 2100. In MIROC and HadGEM2-ES the vegetation changes can mostly be attributed to C4 grass, which grows near the desert margin; in MPI-ESM-LR, C3 trees and C4 grass types are both affected because of the more heterogeneous vegetation composition (Fig. 3).

To attribute the obtained changes to the influences of CO_2 fertilization and precipitation, we investigate how the evolution of precipitation compares to the evolution of vegetation cover in different areas. We thereby distinguish the western and central to eastern Sahel as indicated by the black rectangles in Fig. 2. As preindustrial vegetation cover in MPI-ESM-LR already extends more to the north, the largest changes also occur in more northern areas, as in HadGEM2-ES, where they are confined to
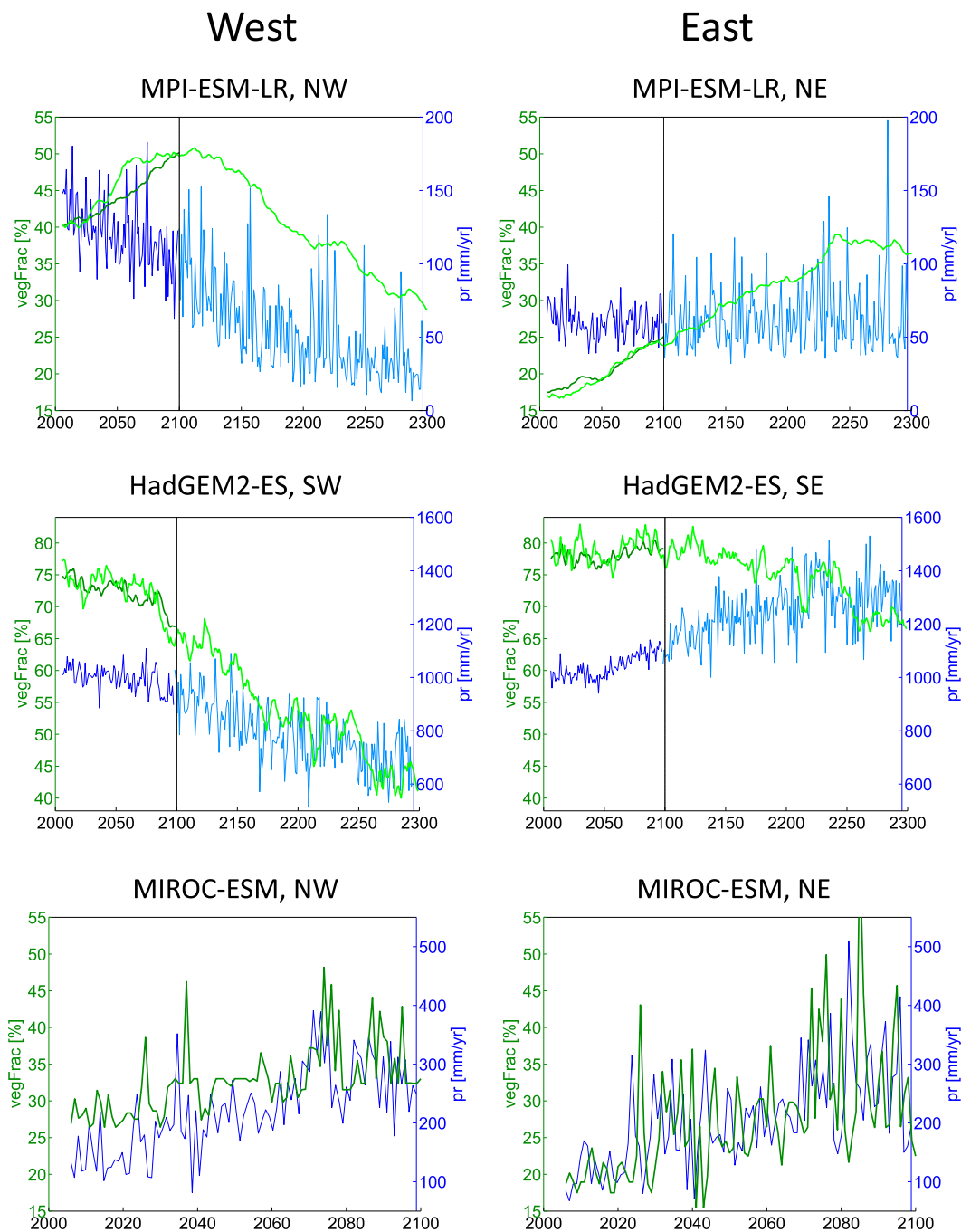
FIG. 4. Temporal evolution of vegetation cover and precipitation in the four areas indicated in Fig. 2: northeast, northwest, southeast, and southwest. The ensemble means of the L2A85 simulations (which end at the black vertical line in 2100) are shown in dark colors, and the extended RCP8.5 simulation is shownin light colors (green shows vegetation cover, and blue shows precipitation). Note that the evolution of vegetation cover before 2100 does not differ qualitatively between the RCP and L2A scenarios.

a comparatively thin latitudinal band. We therefore consider the two northern boxes for MPI-ESM-LR and MIROC-ESM and the two southern boxes for HadGEM2-ES to create time series of the spatial and annual means

(Fig. 4). In addition, we analyze idealized experiments with separated forcings in section 3b.

MPI-ESM-LR and HadGEM2-ES show a similar pattern of precipitation change, most importantly a

progressive drying in the west and a wettening in the southeast of northern Africa. In the long term, vegetation cover roughly follows the trend in precipitation (Fig. 4). However, in MPI-ESM-LR, vegetation cover in the western Sahel increases until somewhat after 2100 in RCP8.5, whereas precipitation decreases. In this initial phase, CO_2 fertilization appears to be the driver of the Sahel greening (also apparent in the northeastern box until 2230). Another exception occurs in HadGEM2-ES in the southeastern box where vegetation cover decreases despite the increase in precipitation (and CO_2) after 2100 as a result of the high temperature at certain grid points (an effect to be discussed in section 3b).

MPI-ESM-LR and HadGEM2-ES agree on the trends and their geographical pattern but disagree on the timing because CO_2 fertilization is stronger in MPI-ESM-LR. In contrast, the greening in MIROC-ESM very closely follows annual-mean precipitation, which increases substantially over northern Africa. As explained in section 2a, the dynamics of vegetation cover directly result from LAI changes in MIROC-ESM, while a much longer time scale is involved in the other two models. Therefore, the interannual variability is much larger in MIROC-ESM.

As changes in precipitation are such an important driver of vegetation dynamics in the Sahel, it is necessary to expand the view to results from other models at this point. Compared to the ensemble of CMIP5 and also previous CMIP3 models, the tendency of a drying in the western and a wettening of the more eastern Sahel like in HadGEM2-ES and MPI-ESM-LR can also be seen in other models. The reason for these tendencies is a shift in the seasonal distribution of rain: The majority of the coupled climate models show a delayed rainy season, which leads to a drying in spring (Biasutti and Sobel 2009). In the western Sahel, the spring drying dominates the change in annual rainfall, while in the center and east it is overcompensated for by a wetter autumn (see Figs. 2b and 5 in Biasutti 2013). Consequently, Fontaine et al. (2011) identified a northern shift of the area of moisture flux convergence in the east and center of the African monsoon region in most CMIP3 models under the A1B scenario and no shift or a southern shift in the west. Monerie et al. (2012) attributed the changes in the eastern parts to an intensification of the low-level monsoon flow and the western drying to increased subsidence and moisture flux divergence in higher atmospheric levels. However, as the relevant regional physical processes are not well understood and very crudely represented in global models (Cook 2008; Patricola and Cook 2010; Druyan 2011; Ruti et al. 2011; Fasullo 2012; Knutti and Sedlacek 2013; Roehrig et al. 2013), the overall response of Sahelian rainfall to greenhouse forcing nonetheless remains highly uncertain. Although the large increase in North African

precipitation in MIROC is exceptional, it should therefore not automatically be regarded as less realistic (Cook 2008). Starting with the next section, we will also examine another source of uncertainties: the effect of CO_2 on physiological processes.

b. Separation of radiative and physiological effects of CO_2

To isolate the impacts of physiological effects and radiative forcing on vegetation distribution, we analyze the idealized scenarios RADPHYS, RAD, and PHYS (Table 2). The analysis follows the logic of a factor separation (Stein and Alpert 1993) with physiological effects and radiative forcing as two (conceptually) independent factors. Figure 5 shows the differences in African vegetation cover compared to the preindustrial simulation for each of the three experiments as well as the synergy of the effects. The synergy represents the nonlinearity of the system. In case of vegetation cover, it can be interpreted as the effect of CO_2 fertilization on the climate change impact or, alternatively, the effect of climate change on CO_2 fertilization (Claussen et al. 2013). It becomes obvious that radiative and physiological effects tend to oppose each other in their impact on vegetation cover in the dry subtropical areas. This contrast is most apparent in MPI-ESM-LR (Fig. 5, top). While a decrease in precipitation in all subtropical areas of the region leads to a decreased vegetation cover in RAD, the CO_2 fertilization acts to green the Sahel and the northwestern Sahara as well as the Arabian Peninsula and the Middle East. In the Sahel, the CO_2 fertilization is the dominating effect, as can be seen in RADPHYS. The vegetation expansion in PHYS consists of C3 as well as C4 plants, as their photosynthesis is modeled in a very similar way and because climate change in PHYS is small.

A similar contrast between RAD and PHYS is obtained in HadGEM2-ES (Fig. 5, middle), although the changes in vegetation cover are not as uniform and the net effect depends on the region. In the western Sahel, the climate change dominates the vegetation response and leads to a retreat of vegetation. In the rest of the Sahel, the CO_2 fertilization dominates and causes a greening. The distribution of C3 plants thereby expands, and the belt of C4 plants (Fig. 3) shifts farther north while soil moisture increases south of 13°N. Although precipitation increases in most parts of the central Sahel, climate change acts to decrease vegetation cover, with the exception of a small region to the east of Lake Chad. The reason for this vegetation retreat is probably the very high temperatures (around 33°C), which tend to decrease productivity. Figure 6d illustrates that the vegetation retreat in
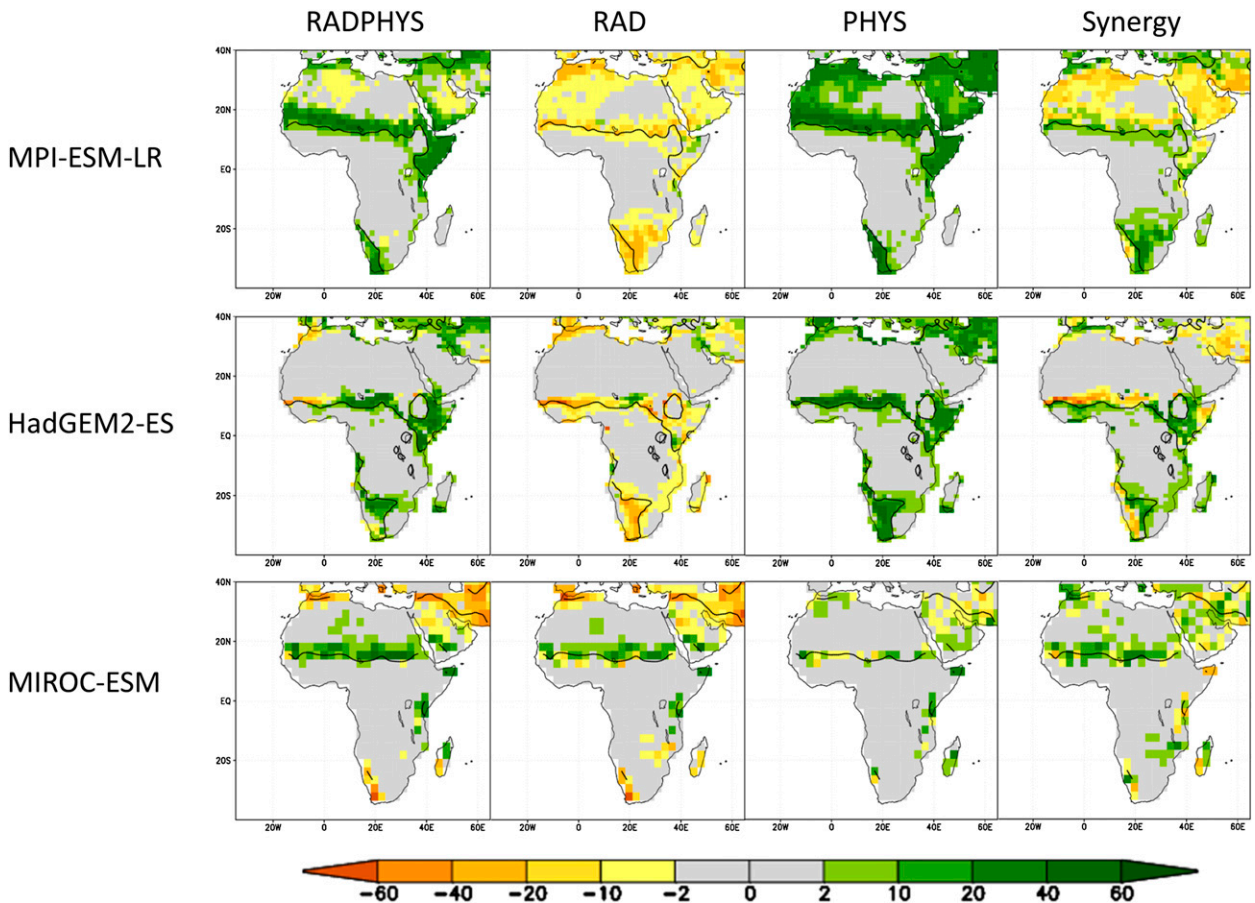
FIG. 5. Differences in vegetation cover (in %) from preindustrial conditions for three idealized scenarios with 1% CO_2 increase per year. Each scenario is averaged over the last 30 yr (years 111–140). RAD stands for the experiment with radiative effects only (CMIP5 name: esmFdbk1), PHYS stands for physiological effects only (esmFixClim1), and RADPHYS stands for the combination of both (1pctCO2). The synergy is calculated as RADPHYS − RAD − PHYS. The black contours mark the boundary of 80% vegetation cover in the preindustrial control simulations (Fig. 1).

areas with increased precipitation is largest where the temperature increase is large and where temperature was already high in the preindustrial climate. Although climate and vegetation are not in equilibrium with each other and with CO_2 at the end of RAD, it is suggestive that the changes cluster in different quadrants in Fig. 6. This effect also explains the vegetation retreat in the RCP8.5 simulation (Fig. 4; HadGEM2-ES, SE). Changes in the seasonal distribution of precipitation could play an additional role.

Hence, MPI-ESM-LR and HadGEM2-ES agree that radiative forcing and CO_2 fertilization are similarly important on the time scale of 100 yr and that a fast increase in CO_2 would green large parts of the Sahel because of an enhanced productivity. However, the longer the climate system can respond to the radiative forcing, the more likely it is that the climate change will counteract this greening, as we showed in section 3a. It is also striking that the synergy of the effects is of a similar magnitude to

the individual effects. In MPI-ESM-LR and HadGEM2-ES, a north–south pattern appears with negative values in the north and positive values in the south. As vegetation cover is limited to values between 0% and 100%, the dependence of vegetation cover on environmental conditions is inevitably nonlinear. Therefore, the synergy as a measure of nonlinearity is potentially large in all areas where vegetation cover comes close to these limits. In particular, the desert regions under preindustrial forcings cannot lose any vegetation when exposed to drying. However, if they become greener as a result of fertilization, the negative climate impact can take effect. At the other end of the scale, where vegetation cover is close to 100%, fertilization can only take little effect, whereas a concurrent drying will allow the fertilization mechanism to become active by keeping vegetation cover high. Therefore, the synergy pattern only reflects the initial vegetation distribution at the desert boundaries.
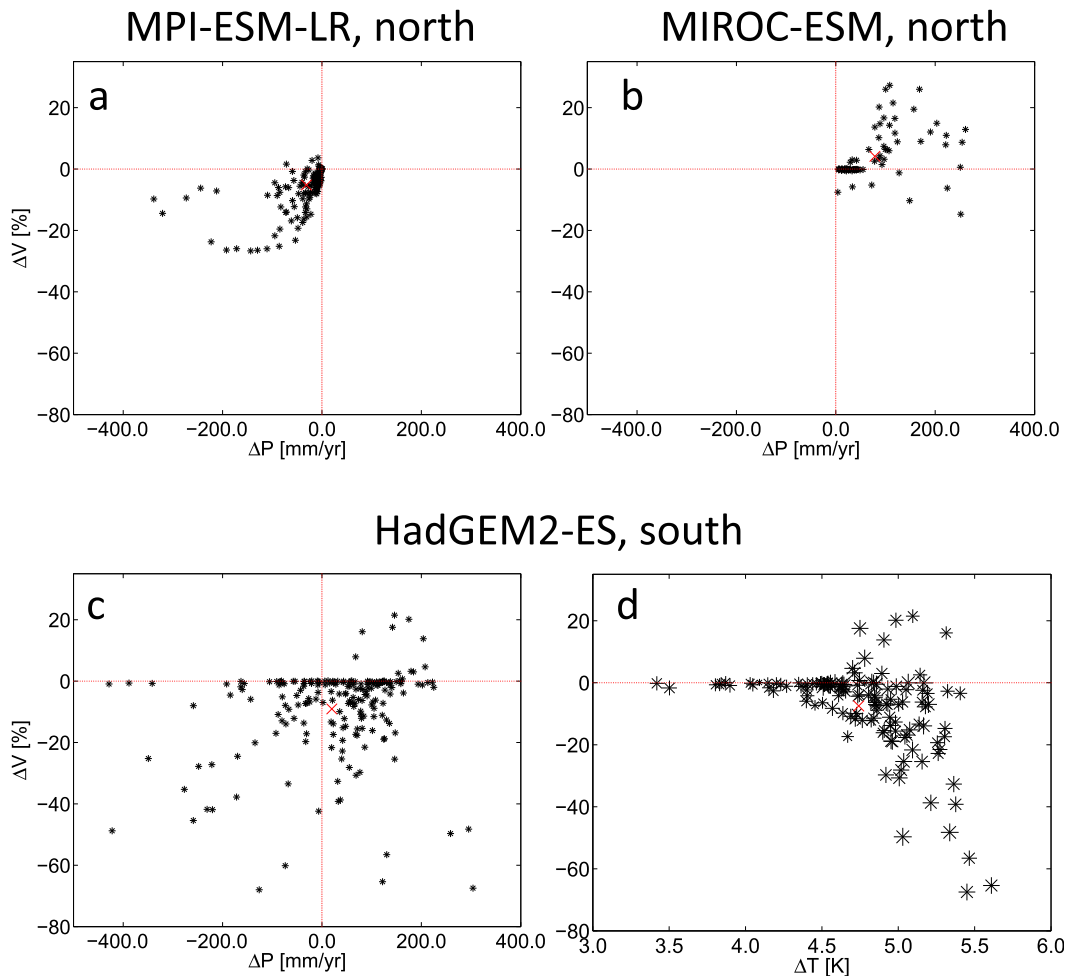
FIG. 6. Relation between (a)–(c) anomalies in vegetation cover and precipitation and between (d) vegetation cover and 2-m air temperature in RAD (difference of last 30 yr from mean preindustrial conditions) in different models. Each cross represents a land grid point within the zone of the desert margin. This zone corresponds to the two northern rectangles in Fig. 2 (13°–24°N) in case of MPI-ESM-LR and MIROC-ESM and to the two southern rectangles (5°–13°N) in case of HadGEM2-ES. In (d) only grid points with a precipitation increase are shown and the size of each cross depends on the preindustrial mean temperature. These preindustrial temperatures range from 16.6°C (smallest crosses) to approximately 30.4°C (largest crosses). Red crosses mark the spatial means of the changes (mean of black crosses in each figure); zero lines are indicated in red.

The results presented so far are not confirmed by the third model under analysis: Fig. 5 (bottom) demonstrates that the greening in MIROC-ESM is almost completely due to climate change: namely, the large increase in precipitation by up to 250 mm over northern Africa. In contrast, the impact of CO_2 fertilization is hardly distinguishable from the pattern of natural variability. Therefore, it becomes obvious that the three models yield similar results because of very different reasons. Figure 6 illustrates these model differences: In MPI-ESM-LR and MIROC-ESM, vegetation cover changes in RAD are both driven by precipitation changes but of different signs. In HadGEM2-ES, the vegetation decrease in RAD cannot be explained with mean precipitation changes

alone (Figs. 6c,d). A hypothetical climate model with a climate response to radiative forcing similar to MPI-ESM-LR or HadGEM2-ES but a response to CO_2 fertilization as weak as MIROC-ESM would show a reduced vegetation growth rather than a greening. In this regard, the multimodel result can hide potential uncertainties. As the processes in the three models are represented so differently, the future development of natural vegetation in the Sahel remains highly uncertain.

c. Impacts of physiological effects on climate

So far, we have discussed climatic and physiological effects separately. This view neglects that there is also a climatic change in the experiment without radiative
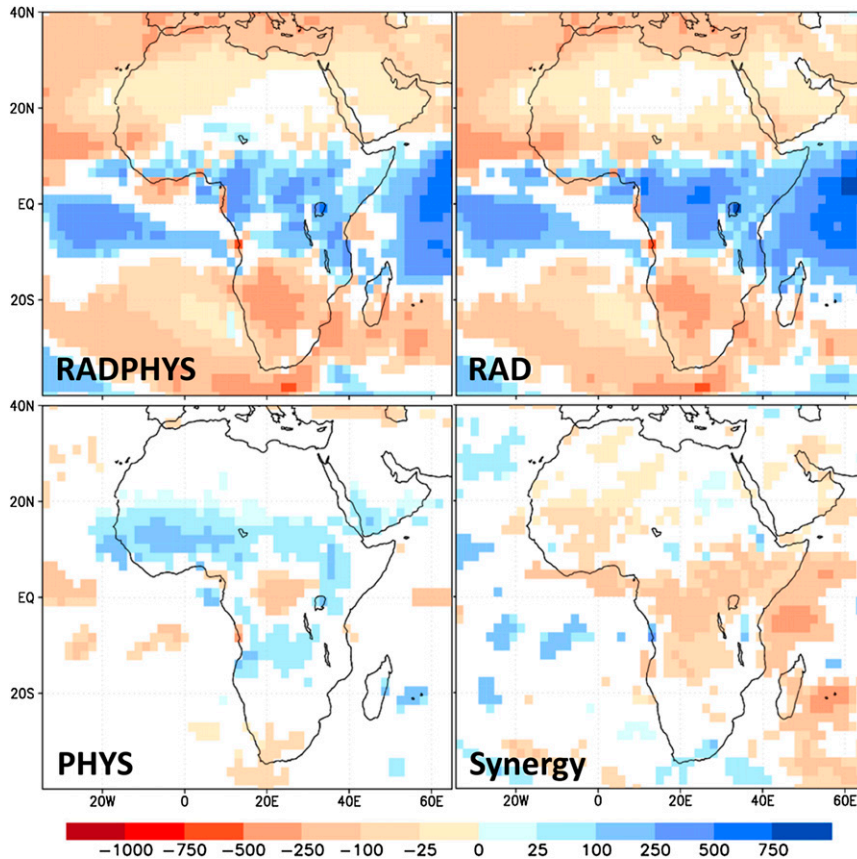
FIG. 7. Factor separation for annual-mean precipitation in MPI-ESM-LR. As in Fig. 5, RADPHYS, RAD, and PHYS show the difference of the last 30 yr from preindustrial conditions. Changes at white grid points are not statistically significant at the 5% level.

forcing (PHYS) because of decreased stomatal conductance and increases in LAI and vegetation cover. PHYS therefore allows us to investigate the potential effects of desert greening on climate in MPI-ESM-LR and HadGEM2-ES. We do not analyze results from MIROC-ESM further because the physiological effect on climate in this model is indiscernible from the natural variability. Compared to the preindustrial simulation, the last 30 yr of PHYS show a global warming of 0.25 K in MPI-ESM-LR and 0.65 K in HadGEM2-ES and reduced evapotranspiration, relative humidity, and cloud cover over land. Globally, this hydrological response is in line with some previous studies (Cox et al. 1999; Betts et al. 2007; Boucher et al. 2009; Cao et al. 2010; Pu and Dickinson 2012).

However, there are regional exceptions to these global changes. First, despite the decrease in stomatal conductance, the vegetation enhances precipitation in the African subtropics, especially in western Africa. Applying the factor separation method to precipitation changes reveals that this effect is of discernible magnitude

when compared to the effect of radiative forcing (Fig. 7): While there are locations with significantly positive, significantly negative, and insignificant precipitation changes in the experiment with combined effects, the contributions of the pure radiative and physiological effects alone are much clearer. While radiative forcing tends to dry the complete Sahel in RAD, physiological effects significantly increase precipitation.

Second, there is a very pronounced tendency of the Sahel not to warm like the rest of the continent (Fig. 8, bottom). To our knowledge, no previous experiment on physiological impacts of CO_2 on climate resulted in a temperature pattern as pronounced as in MPI-ESM-LR and HadGEM2-ES (information and model expansions for previous studies are provided in Table 3): Betts et al. (1997) and Bounoua et al. (2010) obtained substantial effects only in the extratropics, while in Kergoat et al. (2002), Bala et al. (2006), Notaro et al. (2007), and O'ishi et al. (2009) the evapotranspiration change did not dominate the temperature response in the Sahel. In contrast, by forcing the Lund–Potsdam–Jena (LPJ)
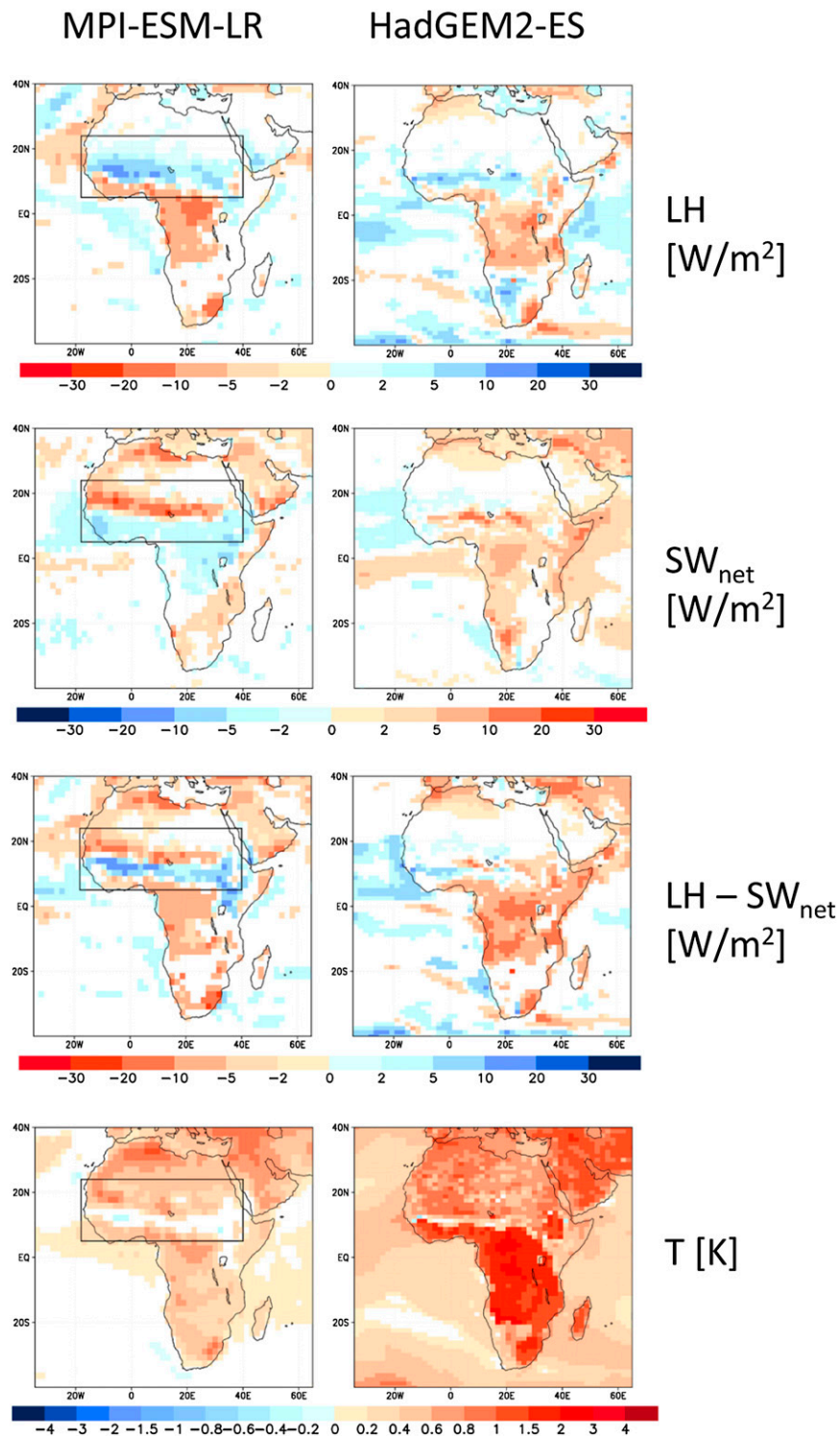
FIG. 8. Impact of the physiological effect on climate in MPI-ESM-LR and HadGEM2-ES. All maps show the last 30 yr in PHYS minus preindustrial mean conditions, as in Figs. 5 and 7. Shown are the surface fluxes of latent heat, net shortwave radiation, their difference, and surface air temperature. LH is defined positive when directed upward. For MPI-ESM-LR, the black rectangle encloses the area analyzed in Fig. 9. Changes at white grid points are not statistically significant at the 5% level.

TABLE 3. Previous studies on physiological effects of CO_2 with implications for the Sahel climate. Specified are the models used in these studies, whether these models allowed for interactive changes in LAI and vegetation cover, and the resulting effects on the Sahel climate compared to the rest of the world.

Study	Model	PHYS scenario	LAI change	Cover change	Effect on Sahel climate
Bala et al. 2006	Integrated Climate and Carbon model (INCCA) [Community Climate Model, version 3.2 (CCM3.2)/Parallel Ocean Program (POP)/Integrated Biosphere Simulator (IBIS)]	SRES A2, prolonged to $4 \times CO_2$	yes	yes	Albedo decrease warms Sahel
Betts et al. 1997	Hadley Centre general circulation model with Sheffield University vegetation model	$2 \times CO_2$	yes	no	Only small changes in tropics
Bounoua et al. 2010	Colorado State University General Circulation Model (GCM)/Simple Biosphere Model, version 2 (SiB2)	$2 \times CO_2$	yes	no	Only small changes in Africa
Kergoat et al. 2002	Unnamed vegetation model, forced with Action de Recherche Petite Echelle Grande Echelle (ARPEGE)	$2 \times CO_2$	yes	no	Effects on ET cancel
Leipprand and Gerten 2006	Lund–Potsdam–Jena (LPJ) (driven by observed climate)	$2 \times CO_2$	yes	yes	Structural effect increases transpiration in arid regions
Notaro et al. 2007	Fast Ocean Atmosphere Model (FOAM)/LPJ	1% increase per year to $4 \times CO_2$	yes	yes	In dry regions, ET does not decrease as elsewhere
O'ishi et al. 2009	MIROC-LPJ	$4 \times CO_2$	yes	yes	Albedo decrease warms semiarid tropics
Cao et al. 2010	NCAR (CCSM3)	$2 \times CO_2$	no	no	More soil evaporation cools eastern Sahel
Gopalakrishnan et al. 2011	NCAR [Community Land Model (CLM) 3.5 driven by observed climate]	various fixed levels of CO_2	no	no	Warming, as everywhere
Pu and Dickinson 2012	NCAR (CCSM4)	$2 \times CO_2$	yes/no	no	Sahel remains cool because of increased ET, especially with LAI increase
Andrews et al. 2011	Hadley Centre Coupled Model, version 3, low resolution with carbon cycle (HadCM3LC)	$4 \times CO_2$	not specified	not specified	Warming, as everywhere
Boucher et al. 2009	HadCM3	IS92a	no	no	No exception in Sahel
Doutriaux-Boucher et al. 2009	HadCM3LC	$2 \times CO_2$	not specified	not specified	Warming, as everywhere
Joshi and Gregory 2008	Hadley Centre Slab Climate Model, version 3 (HadSM3)	$2 \times CO_2$	not specified	no	Colder Sahel when normalized with zonal mean ocean temperature

vegetation model with observed atmospheric data, Leipprand and Gerten (2006) obtain an increased evapotranspiration (although no maps are shown in their study).

When comparing the CMIP5 temperature anomalies to the changes of vegetation cover in Figs. 2 and 5, it is apparent that the cool stripe of the Sahel coincides with the preindustrial border of vegetation cover. South of this transition region, the decrease of stomatal conductance leads to a warming. In previously bare regions north of the cool belt, the lower albedo of the surface increases temperature because of more absorbed shortwave radiation. As the latent heat flux (LH) and net shortwave radiation (SW_{net}) are the terms with the largest changes, their superposition coincides well with the pattern of temperature anomalies (Fig. 8).

In the case of MPI-ESM-LR, the physiological effects of CO_2 on the surface energy balance in different regions becomes obvious in scatter diagrams because the transition region is wider than in HadGEM2-ES. Considering all grid points in the four boxes of Fig. 2 where the preindustrial vegetation cover is above 80%, the anomalies of temperature and latent heat flux are closely related (Fig. 9a). No such relation exists between temperature and absorbed shortwave radiation. When only considering grid points where preindustrial vegetation cover is below 80%, the opposite is true. Figures 9e–h reveal why this occurs by showing changes in LAI on the horizontal axis. In the vegetated areas with small changes in LAI, the reduced stomatal conductance dominates and decreases LH. However, the larger the increase in LAI, the more positive the anomaly becomes. As the bare ground fraction in these initially vegetated areas is low, an increased LAI has comparatively little influence on the surface albedo and thus SW_{net}. In the areas with an initially substantial fraction of desert, the expansion of vegetation into these bare regions causes an albedo decrease. Although LH also tends to increase with increasing LAI in these areas, the absorbed shortwave radiation dominates the surface energy balance.

However, the latent heat-induced cooling in the Sahel can be caused not only by the local vegetation cover change, but also by remote effects. For example, the climate change in the extratropics can lead to a shift in circulation and thus a precipitation increase in the Sahel. Even without any change in local LAI, the increase in precipitation may lead to latent heat cooling. This effect may explain the results by Cao et al. (2010) and Pu and Dickinson (2012), who applied different versions of the National Center for Atmospheric Research (NCAR) Community Climate System Model (CCSM) where no LAI change was permitted (Table 3). Consequently, an offline experiment with prescribed atmospheric conditions with the NCAR land surface model CLM3.5 does not show any increase in evapotranspiration (Gopalakrishnan et al. 2011).

The mechanism of precipitation-induced cooling also becomes apparent in HadGEM2 (called HadGEM2-A in this setup) in two sstClim experiments where both effects of CO_2, radiative and physiological, are active (Table 2). As the temperature contrast between land and ocean is artificially increased in sstClim4xCO2 because of the fixed SSTs, there is a massive increase in precipitation over sub-Saharan Africa (Fig. 10). This precipitation increase causes regionally very different responses in latent heat flux: Where forest coverage is high, the stomatal response causes a decrease in LH. In the subtropics, where LH is most limited by precipitation, an increase occurs that is large enough to decrease surface air temperature in some locations despite the very large longwave heating. A similar effect on Sahel hydrology is obtained by Andrews et al. (2012), who show that a $2 \times CO_2$ experiment with fixed SSTs leads to an exceptional increase in relative humidity in the Sahel (see their Fig. 4e). In HadGEM2, the evaporative cooling occurs despite negligible changes in the vegetation's condition: All plant functional types are fixed to the same distribution in sstClim4xCO2 and sstClim, and LAI shows only very small differences. In MPI-ESM-LR, a large LAI increase occurs between the equator and approximately 17°N, as the phenology of raingreen plant types in JSBACH is sensitive to soil moisture and NPP. Therefore, the remote and local causes of the evaporative cooling in sstClim4xCO2 cannot be strictly separated in MPI-ESM-LR.

Although an attribution of the cool Sahel to the local vegetation change in the PHYS experiment is also not strictly possible, we argue that this local effect is probably more important than remotely induced changes. In the case of HadGEM2-ES, Boucher et al. (2009) obtained a warming that was largest over the forest areas but not a particularly cool Sahel when they prescribed LAI in a previous model version. A similar response was obtained by Doutriaux-Boucher et al. (2009) and Andrews et al. (2011), who only analyze the first 5 yr after an instantaneous CO_2 increase. Assuming that the differences to the CMIP5 results presented in Fig. 8 and the latter three studies are not due to model differences other than the effect of changes in LAI or vegetation cover, the CMIP5 results suggest that vegetation dynamics are of particular importance in the Sahel. However, the northward shift of the ITCZ over the Atlantic in PHYS implies that vegetation dynamics in other regions may also have an effect. Whether an increase in precipitation at a particular grid point is induced by the local vegetation or by the vegetation cover changes elsewhere is therefore hard to separate
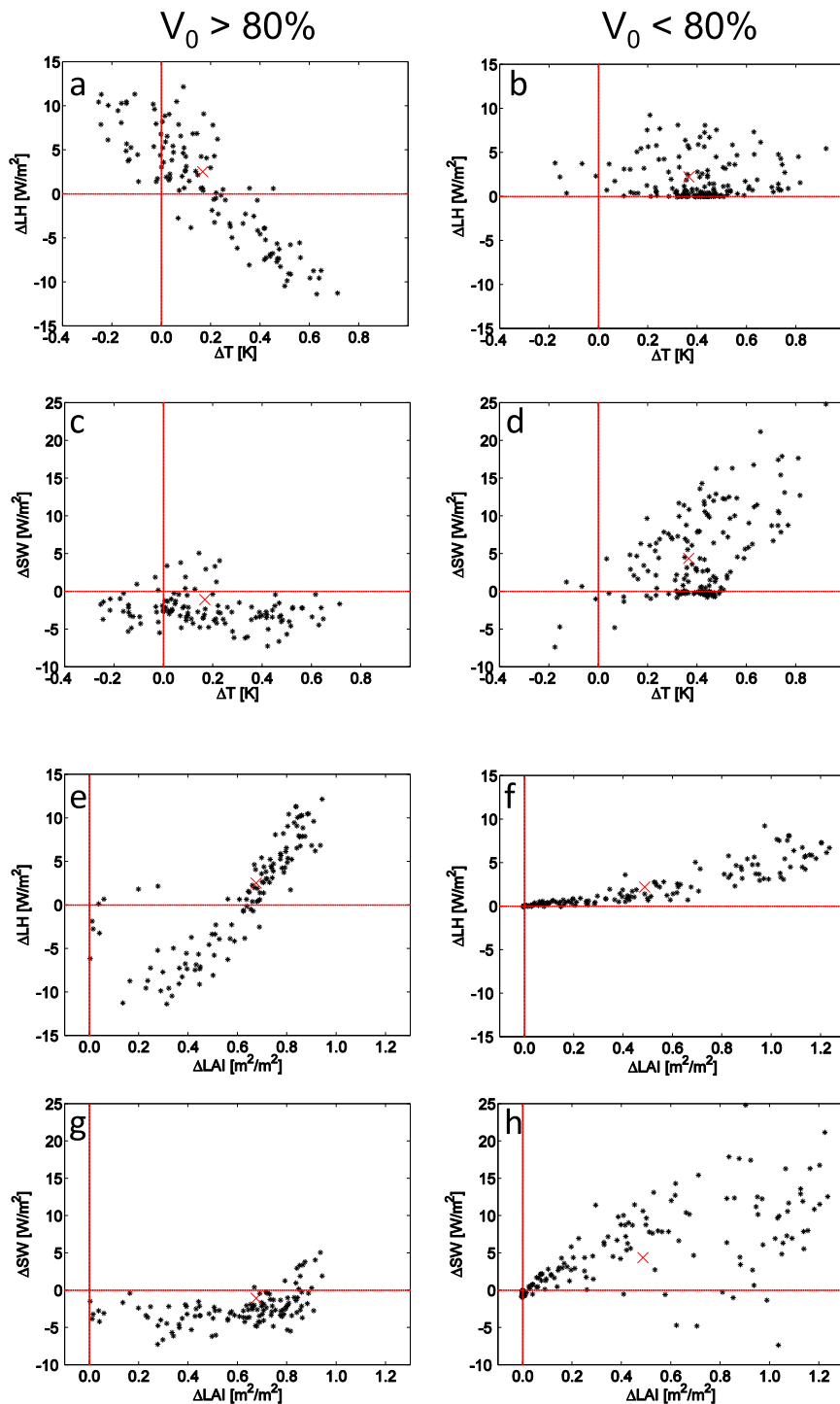
FIG. 9. Relation between anomalies in latent heat flux, surface net shortwave energy, and (a)–(d) surface air temperature and (e)–(h) leaf area index in PHYS (difference from preindustrial conditions) in MPI-ESM-LR. Each cross represents a land grid point within the black rectangle in Fig. 8 (identical to the four boxes in Fig. 2), but separated into areas where preindustrial vegetation cover is (left) above 80% and (right) below 80%. Red crosses mark the spatial means of the changes (mean of black crosses); zero lines are indicated in red.
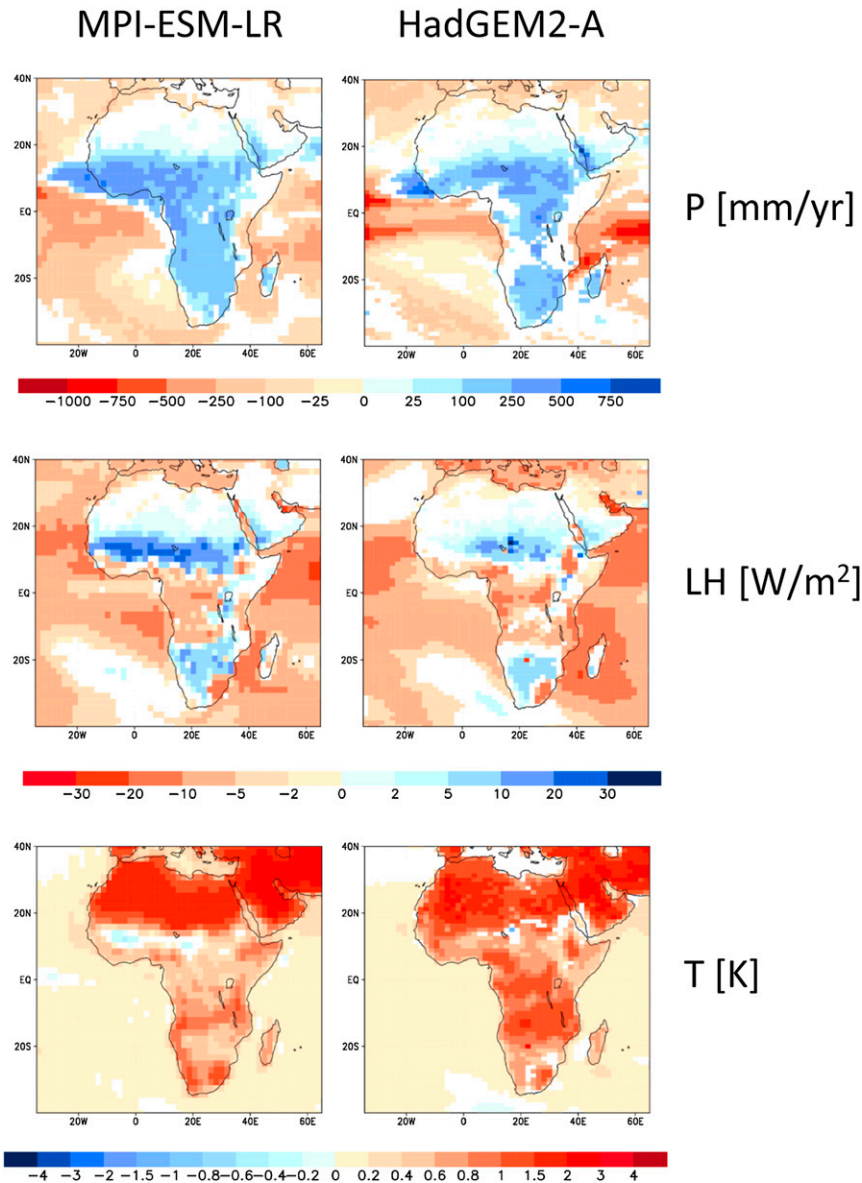
FIG. 10. Time-mean differences between sstClim4xCO2 and sstClim in (left) MPI-ESM-LR and (right) HadGEM2-A. (top) Precipitation, (middle) latent heat flux (positive when directed from land to atmosphere), and (bottom) surface air temperature. Changes at white grid points are not statistically significant at the 5% level.

in HadGEM2-ES. In case of MPI-ESM-LR, it is obvious from Figs. 5, 8, and 9 that latent cooling is strongest in regions where vegetation cover change is largest (under the precondition that initial vegetation cover is already large). Finally, as we know that CO_2 fertilization is large in MPI-ESM-LR and, as precipitation changes are stronger over land than over the ocean, we expect the vegetation expansion to be caused by the local effect rather than by teleconnections. We therefore conclude that vegetation dynamics and structural changes are of particular importance in the Sahel in MPI-ESM-LR.

4. Conclusions

We have shown that three CMIP5 ESMs with dynamic vegetation indicate a Sahel greening due to increased CO_2 until 2100. However, the reason for this change differs among the models. In MIROC-ESM, the greening is the result of an increased precipitation in North Africa. In MPI-ESM-LR, it is the result of CO_2 fertilization. In HadGEM2-ES, there is only little vegetation cover change in the first decades, while a subsequent decrease in rainfall and the large temperatures

initiate a retreat of vegetation in case of the very high CO_2 levels of the RCP8.5 scenario. In MPI-ESM-LR and HadGEM2-ES, there is a tendency of a vegetation retreat in the west of North Africa. In MPI-ESM-LR this retreat does not start until 2100, when climate change proceeds while the fertilization effect levels off because of the stabilized CO_2 concentration. The dependency of vegetation anomalies on the time horizon would probably be even more problematic in a scenario with a CO_2 concentration that is reduced after a large peak (implying very low emissions or even anthropogenic carbon removal activities). Under such conditions, the fertilization effect would decrease with the concentrations, while the committed climate change from the high-emission period would also act to reduce the vegetation's productivity. The impact of CO_2 would then tend to resemble the RAD scenario.

As there are several important drivers of vegetation changes in the Sahel that can oppose each other and are insufficiently understood and modeled, the three models only represent three trajectories that do not represent the full spectrum of possibilities. In particular, improved parameterizations of surface and boundary layer processes, tropical convection, and mesoscale systems are crucial to better represent Sahelian rainfall in climate models (Pohl and Douville 2011; Ruti et al. 2011; Fasullo 2012; Rowell 2012; Roehrig et al. 2013). Considering the large spatial gradients and the importance of small-scale features and land–atmosphere coupling of the Sahel region, in combination with the scarcity of observations, progress may remain slow, and the application of regional models may be of particular benefit (Cook 2008; Patricola and Cook 2010).

As many global models project rather small changes in annual rainfall (Biasutti 2013), it seems likely that physiological effects of CO_2 will be of particular importance and a further source of uncertainty considering the low level of understanding of these effects on long time scales (Field et al. 1995; Long et al. 2004; Norby and Zak 2011; Reich and Hobbie 2013). The idealized factor separation experiments of CMIP5 indicate that CO_2 fertilization is one of the dominating drivers of vegetation cover changes in MPI-ESM-LR and HadGEM2-ES, which is similar to earlier results performed with FOAM-LPJ by Notaro et al. (2007).

It also seems clear that such structural vegetation changes affect the Sahelian climate, although the relative importance of changes in albedo and evapotranspiration is inconsistent among models. As several studies showed similar effects on both aspects of the energy balance, we consider it likely that previous experiments could not reveal the spatial separation of mechanisms because of their lower resolution. However, the balance of effects depends on the physical properties of plants, represented as constant parameters of plant functional types (PFTs) in current models. Also, the translation of changes of productivity on a leaf level and short time scales into the dynamics of vegetation distribution and composition over centuries remains a major uncertainty. To isolate the climatic effect of local vegetation changes from teleconnections, it may be of value in the future to perform additional simulations with an offline land model where precipitation is prescribed (similar to Gopalakrishnan et al. 2011), to compare simulations with and without structural vegetation changes (as, e.g., in Betts et al. 1997), or to allow dynamic vegetation only in some regions of the world but not in others.

The CMIP5 results also have implications for previously used concepts of analysis: First, it is a common practice to analyze the difference between RADPHYS and RAD experiments to determine the physiological effects (Andrews et al. 2011; Betts et al. 1997; Bounoua et al. 2010; Levis et al. 1999, 2000; Doutriaux-Boucher et al. 2009; Joshi and Gregory 2008; O'ishi et al. 2009). The substantial synergy effect implies that this difference is not identical to the pure PHYS effect. While the chosen approach may make no difference for fast effects such as stomata closure, it leads to differences whenever large changes in vegetation cover occur. Differences will appear mainly in those quantities that are much affected by vegetation cover. Of course, the question of which approach is more appropriate depends on the aim of the analysis. To determine the additional contribution of physiology on climate change, analyzing RADPHYS − RAD appears to be an appropriate approach.

Second, the concept of climate forcings (in terms of $W\,m^{-2}$) and feedbacks (in terms of $W\,m^{-2}\,K^{-1}$) is questioned when physiological effects are important. The fast processes of nonradiative forcing (stomatal closure and subsequent changes in cloud cover) are usually added to radiatively induced adjustments: for example, adjustments of stratospheric temperature, lapse rate, and cloud cover (Andrews and Forster 2008; Andrews et al. 2012). However, the slow structural responses of vegetation to enhanced CO_2 are not related to temperature-driven feedbacks (Bony et al. 2006) and must conceptually also be regarded as forcing adjustments that are so slow that they cannot be separated from climate feedbacks. As CO_2 contributes most to the anthropogenic radiative forcing and, as climate change and CO_2-driven vegetation dynamics evolve on similar time scales, it can be argued that CO_2-induced vegetation cover changes can conceptually be formulated as a climate feedback (Cao et al. 2010). However, the CMIP5 results indicate the limits of this assumption, as changes in LAI and vegetation distribution are faster than the warming of the deep ocean.

Third, it has been speculated whether land–atmosphere feedbacks in North Africa can cause abrupt transitions (Claussen et al. 1999; deMenocal et al. 2000) or even multiple equilibria (Brovkin et al. 1998). Although the feedback appears to be too small to allow for such non-linear effects in current ESMs, CO_2 fertilization may make the region more susceptible to precipitation changes than in the past.

REFERENCES

Ackerley, D., B. B. B. Booth, S. H. E. Knight, E. J. Highwood, D. J. Frame, M. R. Allen, and D. P. Rowell, 2011: Sensitivity of twentieth-century Sahel rainfall to sulfate aerosol and CO_2 forcing. *J. Climate,* **24,** 4999–5014, doi:10.1175/JCLI-D-11-00019.1.

Ainsworth, E. A., and S. P. Long, 2005: What have we learned from 15 years of free-air CO_2 enrichment (FACE)? A meta-analytic review of the responses of photosynthesis, canopy properties and plant production to rising CO_2. *New Phytol.,* **165,** 351–372, doi:10.1111/j.1469-8137.2004.01224.x.

——, and A. Rogers, 2007: The response of photosynthesis and stomatal conductance to rising $[CO_2]$: Mechanisms and environmental interactions. *Plant Cell Environ.,* **30,** 258–270, doi:10.1111/j.1365-3040.2007.01641.x.

Andrews, T., and P. M. Forster, 2008: CO_2 forcing induces semidirect effects with consequences for climate feedback interpretations. *Geophys. Res. Lett.,* **35,** L04802, doi:10.1029/2007GL032273.

——, M. Doutriaux-Boucher, O. Boucher, and P. M. Forster, 2011: A regional and global analysis of carbon dioxide physiological forcing and its impact on climate. *Climate Dyn.,* **36,** 783–792, doi:10.1007/s00382-010-0742-1.

——, J. Gregory, P. M. Forster, and M. J. Webb, 2012: Cloud adjustment and its role in CO_2 radiative forcing and climate sensitivity: A review. *Surv. Geophys.,* **33,** 619–635, doi:10.1007/s10712-011-9152-0.

Anyamba, A., and C. Tucker, 2005: Analysis of Sahelian vegetation dynamics using NOAA-AVHRR NDVI data from 1981–2003. *J. Arid Environ.,* **63,** 596–614, doi:10.1016/j.jaridenv.2005.03.007.

Arora, V. K., and Coauthors, 2013: Carbon–concentration and carbon–climate feedbacks in CMIP5 Earth system models. *J. Climate,* **26,** 5289–5314, doi:10.1175/JCLI-D-12-00494.1.

Bala, G., K. Caldeira, A. Mirin, M. Wickett, C. Delire, and T. J. Phillips, 2006: Biogeophysical effects of CO_2 fertilization on global climate. *Tellus,* **58B,** 620–627, doi:10.1111/j.1600-0889.2006.00210.x.

Ball, J., I. Woodrow, and J. Berry, 1987: A model predicting stomatal conductance and its contribution to the control of photosynthesis under different environmental conditions. *Progress in Photosynthesis Research,* J. Biggins, Ed., Springer Netherlands, 221–224, doi:10.1007/978-94-017-0519-6_48.

Betts, R. A., P. M. Cox, S. E. Lee, and F. I. Woodward, 1997: Contrasting physiological and structural vegetation feedbacks in climate change simulations. *Nature,* **387,** 796–799, doi:10.1038/42924.

——, and Coauthors, 2007: Projected increase in continental runoff due to plant responses to increasing carbon dioxide. *Nature,* **448,** 1037–1041, doi:10.1038/nature06045.

Biasutti, M., 2013: Forced Sahel rainfall trends in the CMIP5 archive. *J. Geophys. Res. Atmos.,* **118,** 1613–1623, doi:10.1002/jgrd.50206.

——, and A. H. Sobel, 2009: Delayed Sahel rainfall and global seasonal cycle in a warmer climate. *Geophys. Res. Lett.,* **36,** L23707, doi:10.1029/2009GL041303.

——, I. M. Held, A. H. Sobel, and A. Giannini, 2008: SST forcings and Sahel rainfall variability in simulations of the twentieth and twenty-first centuries. *J. Climate,* **21,** 3471–3486, doi:10.1175/2007JCLI1896.1.

Bony, S., and Coauthors, 2006: How well do we understand and evaluate climate change feedback processes? *J. Climate,* **19,** 3445–3482, doi:10.1175/JCLI3819.1.

Boucher, O., A. Jones, and R. A. Betts, 2009: Climate response to the physiological impact of carbon dioxide on plants in the Met Office Unified Model HadCM3. *Climate Dyn.,* **32,** 237–249, doi:10.1007/s00382-008-0459-6.

Bounoua, L., F. G. Hall, P. J. Sellers, A. Kumar, G. J. Collatz, C. J. Tucker, and M. L. Imhoff, 2010: Quantifying the negative feedback of vegetation to greenhouse warming: A modeling approach. *Geophys. Res. Lett.,* **37,** L23701, doi:10.1029/2010GL045338.

Brovkin, V., M. Claussen, V. Petoukhov, and A. Ganopolski, 1998: On the stability of the atmosphere-vegetation system in the Sahara/Sahel region. *J. Geophys. Res.,* **103,** 31 613–31 624, doi:10.1029/1998JD200006.

——, T. Raddatz, C. H. Reick, M. Claussen, and V. Gayler, 2009: Global biogeophysical interactions between forest and climate. *Geophys. Res. Lett.,* **36,** L07405, doi:10.1029/2009GL037543.

——, L. Boysen, T. Raddatz, V. Gayler, A. Loew, and M. Claussen, 2013a: Evaluation of vegetation cover and land-surface albedo in MPI-ESM CMIP5 simulations. *J. Adv. Model. Earth Syst.,* **5,** 48–57, doi:10.1029/2012MS000169.

——, and Coauthors, 2013b: Effect of anthropogenic land-use and land-cover changes on climate and land carbon storage in CMIP5 projections for the twenty-first century. *J. Climate,* **26,** 6859–6881, doi:10.1175/JCLI-D-12-00623.1.

Cao, L., G. Bala, K. Caldeira, R. Nemani, and G. Ban-Weiss, 2010: Importance of carbon dioxide physiological forcing to future

climate change. *Proc. Natl. Acad. Sci. USA,* **107,** 9513–9518, doi:10.1073/pnas.0913000107.

Charney, J., 1975: Dynamics of deserts and drought in the Sahel. *Quart. J. Roy. Meteor. Soc.,* **101,** 193–202, doi:10.1002/qj.49710142802.

——, P. H. Stone, and W. J. Quirk, 1975: Drought in the Sahara: A biogeophysical feedback mechanism. *Science,* **187,** 434–435, doi:10.1126/science.187.4175.434.

——, W. Quirk, S. Chow, and J. Kornfield, 1977: A comparative study of the effects of albedo change on drought in semi-arid regions. *J. Atmos. Sci.,* **34,** 1366–1385, doi:10.1175/1520-0469(1977)034<1366:ACSOTE>2.0.CO;2.

Chou, C., and J. D. Neelin, 2004: Mechanisms of global warming impacts on regional tropical precipitation. *J. Climate,* **17,** 2688–2701, doi:10.1175/1520-0442(2004)017<2688:MOGWIO>2.0.CO;2.

——, ——, C.-A. Chen, and J.-Y. Tu, 2009: Evaluating the "rich-get-richer" mechanism in tropical precipitation change under global warming. *J. Climate,* **22,** 1982–2005, doi:10.1175/2008JCLI2471.1.

Claussen, M., 1997: Modeling bio-geophysical feedback in the African and Indian monsoon region. *Climate Dyn.,* **13,** 247–257, doi:10.1007/s003820050164.

——, 2009: Late Quaternary vegetation–climate feedbacks. *Climate Past,* **5,** 203–216, doi:10.5194/cp-5-203-2009.

——, C. Kubatzki, V. Brovkin, A. Ganopolski, P. Hoelzmann, and H. J. Pachur, 1999: Simulation of an abrupt change in Saharan vegetation in the mid-Holocene. *Geophys. Res. Lett.,* **26,** 2037–2040, doi:10.1029/1999GL900494.

——, V. Brovkin, A. Ganopolski, C. Kubatzki, and V. Petoukhov, 2003: Climate change in northern Africa: The past is not the future. *Climatic Change,* **57,** 99–118, doi:10.1023/A:1022115604225.

——, K. Selent, V. Brovkin, T. Raddatz, and V. Gayler, 2013: Impact of CO_2 and climate on Last Glacial Maximum vegetation—A factor separation. *Biogeosciences,* **10,** 3593–3604, doi:10.5194/bg-10-3593-2013.

Collatz, G. J., J. T. Ball, C. Grivet, and J. A. Berry, 1991: Physiological and environmental regulation of stomatal conductance, photosynthesis and transpiration: A model that includes a laminar boundary layer. *Agric. For. Meteor.,* **54,** 107–136, doi:10.1016/0168-1923(91)90002-8.

——, M. Ribas-Carbo, and J. A. Berry, 1992: Coupled photosynthesis-stomatal conductance model for leaves of C_4 plants. *Aust. J. Plant Physiol.,* **19,** 519–538, doi:10.1071/PP9920519.

Collins, W. J., and Coauthors, 2011: Development and evaluation of an Earth-system model—HadGEM2. *Geosci. Model Dev.,* **4,** 1051–1075, doi:10.5194/gmd-4-1051-2011.

Cook, K. H., 2008: Climate science: The mysteries of Sahel droughts. *Nat. Geosci.,* **1,** 647–648, doi:10.1038/ngeo320.

Cox, P. M., 2001: Description of the "TRIFFID" dynamic global vegetation model. Met Office Hadley Centre Tech. Note 24, 16 pp. [Available online at http://www.metoffice.gov.uk/media/pdf/9/h/HCTN_24.pdf.]

——, R. A. Betts, C. B. Bunton, R. L. H. Essery, P. R. Rowntree, and J. Smith, 1999: The impact of new land surface physics on the GCM simulation of climate and climate sensitivity. *Climate Dyn.,* **15,** 183–203, doi:10.1007/s003820050276.

de Jong, R., J. Verbesselt, M. E. Schaepman, and S. de Bruin, 2012: Trend changes in global greening and browning: Contribution of short-term trends to longer-term change. *Global Change Biol.,* **18,** 642–655, doi:10.1111/j.1365-2486.2011.02578.x.

deMenocal, P., J. Ortiz, T. Guilderson, J. Adkins, M. Sarnthein, L. Baker, and M. Yarusinsky, 2000: Abrupt onset and termination of the African Humid Period: Rapid climate responses to gradual insolation forcing. *Quat. Sci. Rev.,* **19,** 347–361, doi:10.1016/S0277-3791(99)00081-5.

Donohue, R. J., M. L. Roderick, T. R. McVicar, and G. D. Farquhar, 2013: Impact of CO_2 fertilization on maximum foliage cover across the globe's warm, arid environments. *Geophys. Res. Lett.,* **40,** 3031–3035, doi:10.1002/grl.50563.

Doutriaux-Boucher, M., M. J. Webb, J. M. Gregory, and O. Boucher, 2009: Carbon dioxide induced stomatal closure increases radiative forcing via a rapid reduction in low cloud. *Geophys. Res. Lett.,* **36,** L02703, doi:10.1029/2008GL036273.

Druyan, L. M., 2011: Studies of 21st-century precipitation trends over West Africa. *Int. J. Climatol.,* **31,** 1415–1424, doi:10.1002/joc.2180.

Essery, R. L. H., M. J. Best, R. A. Betts, P. M. Cox, and C. M. Taylor, 2003: Explicit representation of subgrid heterogeneity in a GCM land surface scheme. *J. Hydrometeor.,* **4,** 530–543, doi:10.1175/1525-7541(2003)004<0530:EROSHI>2.0.CO;2.

Farquhar, G., S. von Caemmerer, and J. Berry, 1980: A biochemical model of photosynthetic CO_2 assimilation in leaves of C_3 species. *Planta,* **149,** 78–90, doi:10.1007/BF00386231.

Fasullo, J., 2012: A mechanism for land–ocean contrasts in global monsoon trends in a warming climate. *Climate Dyn.,* **39,** 1137–1147, doi:10.1007/s00382-011-1270-3.

Fensholt, R., and K. Rasmussen, 2011: Analysis of trends in the Sahelian 'rain-use efficiency' using GIMMS NDVI, RFE and GPCP rainfall data. *Remote Sens. Environ.,* **115,** 438–451, doi:10.1016/j.rse.2010.09.014.

Field, C. B., R. B. Jackson, and H. A. Mooney, 1995: Stomatal responses to increased CO_2: Implications from the plant to the global scale. *Plant Cell Environ.,* **18,** 1214–1225, doi:10.1111/j.1365-3040.1995.tb00630.x.

Fontaine, B., P. Roucou, and P.-A. Monerie, 2011: Changes in the African monsoon region at medium-term time horizon using 12 AR4 coupled models under the A1b emissions scenario. *Atmos. Sci. Lett.,* **12,** 83–88, doi:10.1002/asl.321.

Giannini, A., 2010: Mechanisms of climate change in the semiarid African Sahel: The local view. *J. Climate,* **23,** 743–756, doi:10.1175/2009JCLI3123.1.

——, R. Saravanan, and P. Chang, 2003: Oceanic forcing of Sahel rainfall on interannual to interdecadal time scales. *Science,* **302,** 1027–1030, doi:10.1126/science.1089357.

Giorgetta, M. A., and Coauthors, 2013: Climate and carbon cycle changes from 1850 to 2100 in MPI-ESM simulations for the Coupled Model Intercomparison Project phase 5. *J. Adv. Model. Earth Syst.,* **5,** 572–597, doi:10.1002/jame.20038.

Gopalakrishnan, R., G. Bala, M. Jayaraman, L. Cao, R. Nemani, and N. H. Ravindranath, 2011: Sensitivity of terrestrial water and energy budgets to CO_2-physiological forcing: An investigation using an offline land model. *Environ. Res. Lett.,* **6,** 044013, doi:10.1088/1748-9326/6/4/044013.

Haarsma, R. J., F. M. Selten, S. L. Weber, and M. Kliphuis, 2005: Sahel rainfall variability and response to greenhouse warming. *Geophys. Res. Lett.,* **32,** L17702, doi:10.1029/2005GL023232.

Hajima, T., T. Ise, K. Tachiiri, E. Kato, S. Watanabe, and M. Kawamiya, 2012: Climate change, allowable emission, and earth system response to representative concentration pathway scenarios. *J. Meteor. Soc. Japan,* **90,** 417–434, doi:10.2151/jmsj.2012-305.

Hansen, M., R. DeFries, J. R. Townshend, M. Carroll, C. Dimiceli, and R. Sohlberg, 2007: Vegetation Continuous Fields MOD44B, 2001 percent tree cover, collection 4. University of Maryland, College Park, MD, digital media. [Available online at http://www.landcover.org/data/vcf/.]

Herceg, D., A. H. Sobel, and L. Sun, 2007: Regional modeling of decadal rainfall variability over the Sahel. *Climate Dyn.,* **29,** 89–99, doi:10.1007/s00382-006-0218-5.

Hoerling, M., J. Hurrell, J. Eischeid, and A. Phillips, 2006: Detection and attribution of twentieth-century northern and southern African rainfall change. *J. Climate,* **19,** 3989–4008, doi:10.1175/JCLI3842.1.

Ilyina, T., K. D. Six, J. Segschneider, E. Maier-Reimer, H. Li, and I. Nuñez-Riboni, 2013: Global ocean biogeochemistry model HAMOCC: Model architecture and performance as component of the MPI-Earth system model in different CMIP5 experimental realizations. *J. Adv. Model. Earth Syst.,* **5,** 287–315, doi:10.1029/2012MS000178.

Jolly, D., S. Harrison, B. Damnati, and R. Bonnefille, 1998a: Simulated climate and biomes of Africa during the late quaternary: Comparison with pollen and lake status data. *Quat. Sci. Rev.,* **17,** 629–657, doi:10.1016/S0277-3791(98)00015-8.

——, and Coauthors, 1998b: Biome reconstruction from pollen and plant macrofossil data for Africa and the Arabian peninsula at 0 and 6000 years. *J. Biogeogr.,* **25,** 1007–1027, doi:10.1046/j.1365-2699.1998.00238.x.

Joly, M., A. Voldoire, H. Douville, P. Terray, and J.-F. Royer, 2007: African monsoon teleconnections with tropical SSTs: Validation and evolution in a set of IPCC4 simulations. *Climate Dyn.,* **29,** 1–20, doi:10.1007/s00382-006-0215-8.

Joshi, M., and J. Gregory, 2008: Dependence of the land–sea contrast in surface climate response on the nature of the forcing. *Geophys. Res. Lett.,* **35,** L24802, doi:10.1029/2008GL036234.

Jungclaus, J. H., and Coauthors, 2013: Characteristics of the ocean simulations in MPIOM, the ocean component of the MPI-Earth system model. *J. Adv. Model. Earth Syst.,* **5,** 422–446, doi:10.1002/jame.20023.

Kergoat, L., S. Lafont, H. Douville, B. Berthelot, G. Dedieu, S. Planton, and J.-F. Royer, 2002: Impact of doubled CO_2 on global-scale leaf area index and evapotranspiration: Conflicting stomatal conductance and LAI responses. *J. Geophys. Res.,* **107,** 4808, doi:10.1029/2001JD001245.

Kim, H.-J., B. Wang, and Q. Ding, 2008: The global monsoon variability simulated by CMIP3 coupled climate models. *J. Climate,* **21,** 5271–5294, doi:10.1175/2008JCLI2041.1.

Knutti, R., and J. Sedlacek, 2013: Robustness and uncertainties in the new CMIP5 climate model projections. *Nat. Climate Change,* **3,** 369–373, doi:10.1038/nclimate1716.

Kutzbach, J. E., 1981: Monsoon climate of the early Holocene: Climate experiment with the earth's orbital parameters for 9000 years ago. *Science,* **214,** 59–61, doi:10.1126/science.214.4516.59.

Leakey, A. D. B., E. A. Ainsworth, C. J. Bernacchi, A. Rogers, S. P. Long, and D. R. Ort, 2009: Elevated CO_2 effects on plant carbon, nitrogen, and water relations: Six important lessons from FACE. *J. Exp. Bot.,* **60,** 2859–2876, doi:10.1093/jxb/erp096.

Leipprand, A., and D. Gerten, 2006: Global effects of doubled atmospheric CO_2 content on evapotranspiration, soil moisture and runoff under potential natural vegetation. *Hydrol. Sci. J.,* **51,** 171–185, doi:10.1623/hysj.51.1.171.

Leuning, R., 1995: A critical appraisal of a combined stomatal-photosynthesis model for C_3 plants. *Plant Cell Environ.,* **18,** 339–355, doi:10.1111/j.1365-3040.1995.tb00370.x.

Levis, S., J. A. Foley, and D. Pollard, 1999: Potential high-latitude vegetation feedbacks on CO_2-induced climate change. *Geophys. Res. Lett.,* **26,** 747–750, doi:10.1029/1999GL900107.

——, ——, and ——, 2000: Large-scale vegetation feedbacks on a doubled CO_2 climate. *J. Climate,* **13,** 1313–1325, doi:10.1175/1520-0442(2000)013<1313:LSVFOA>2.0.CO;2.

Lézine, A.-M., W. Zheng, P. Braconnot, and G. Krinner, 2011: Late Holocene plant and climate evolution at Lake Yoa, northern Chad: Pollen data and climate simulations. *Climate Past,* **7,** 1351–1362, doi:10.5194/cp-7-1351-2011.

Long, S. P., E. A. Ainsworth, A. K. Rogers, and D. R. Ort, 2004: Rising atmospheric carbon dioxide: Plants FACE the future. *Annu. Rev. Plant Biol.,* **55,** 591–628, doi:10.1146/annurev.arplant.55.031903.141610.

Lu, J., and T. L. Delworth, 2005: Oceanic forcing of late 20th century Sahel drought. *Geophys. Res. Lett.,* **32,** L22706, doi:10.1029/2005GL023316.

Mahowald, N. M., 2007: Anthropocene changes in desert area: Sensitivity to climate model predictions. *Geophys. Res. Lett.,* **34,** L18817, doi:10.1029/2007GL030472.

Maier-Reimer, E., I. Kriest, J. Segschneider, and P. Wetzel, 2005: The Hamburg Ocean Carbon Cycle model HAMOCC5.1—Technical description release 1.1. Max Planck Institute Tech. Rep. 14, 57 pp. [Available online at http://www.mpimet.mpg.de/fileadmin/publikationen/erdsystem_14.pdf.]

Martin, G. M., and Coauthors, 2011: The HadGEM2 family of Met Office Unified Model climate configurations. *Geosci. Model Dev.,* **4,** 723–757, doi:10.5194/gmd-4-723-2011.

Meinshausen, M., and Coauthors, 2011: The RCP greenhouse gas concentrations and their extensions from 1765 to 2300. *Climatic Change,* **109,** 213–241, doi:10.1007/s10584-011-0156-z.

Mohino, E., S. Janicot, and J. Bader, 2011: Sahel rainfall and decadal to multi-decadal sea surface temperature variability. *Climate Dyn.,* **37,** 419–440, doi:10.1007/s00382-010-0867-2.

Monerie, P.-A., B. Fontaine, and P. Roucou, 2012: Expected future changes in the African monsoon between 2030 and 2070 using some CMIP3 and CMIP5 models under a medium-low RCP scenario. *J. Geophys. Res.,* **117,** D16111, doi:10.1029/2012JD017510.

Norby, R. J., and D. R. Zak, 2011: Ecological lessons from Free-Air CO_2 Enrichment (FACE) experiments. *Annu. Rev. Ecol. Evol. Syst.,* **42,** 181–203, doi:10.1146/annurev-ecolsys-102209-144647.

Notaro, M., S. Vavrus, and Z. Liu, 2007: Global vegetation and climate change due to future increases in CO_2 as projected by a fully coupled model with dynamic vegetation. *J. Climate,* **20,** 70–90, doi:10.1175/JCLI3989.1.

O'ishi, R., A. Abe-Ouchi, I. C. Prentice, and S. Sitch, 2009: Vegetation dynamics and plant CO_2 responses as positive feedbacks in a greenhouse world. *Geophys. Res. Lett.,* **36,** L11706, doi:10.1029/2009GL038217.

Otterman, J., 1974: Baring high-albedo soils by overgrazing: A hypothesized desertification mechanism. *Science,* **186,** 531–533, doi:10.1126/science.186.4163.531.

Patricola, C. M., and K. H. Cook, 2010: Northern African climate at the end of the twenty-first century: An integrated application of regional and global climate models. *Climate Dyn.,* **35,** 193–212, doi:10.1007/s00382-009-0623-7.

——, and ——, 2011: Sub-Saharan northern African climate at the end of the twenty-first century: Forcing factors and climate change processes. *Climate Dyn.,* **37,** 1165–1188, doi:10.1007/s00382-010-0907-y.

Petit-Maire, N., 1990: Will greenhouse green the Sahara? *Episodes,* **13,** 103–107.

Pitman, A. J., and Coauthors, 2009: Uncertainties in climate responses to past land cover change: First results from the LUCID intercomparison study. *Geophys. Res. Lett.,* **36,** L14814, doi:10.1029/2009GL039076.

Pohl, B., and H. Douville, 2011: Diagnosing GCM errors over West Africa using relaxation experiments. Part I: Summer monsoon climatology and interannual variability. *Climate Dyn.,* **37,** 1293–1312, doi:10.1007/s00382-010-0911-2.

Prentice, I. C., and Coauthors, 2000: Mid-Holocene and glacial-maximum vegetation geography of the northern continents and Africa. *J. Biogeogr.,* **27,** 507–519, doi:10.1046/j.1365-2699.2000.00425.x.

Pu, B., and R. E. Dickinson, 2012: Examining vegetation feedbacks on global warming in the Community Earth System Model. *J. Geophys. Res.,* **117,** D20110, doi:10.1029/2012JD017623.

Raddatz, T., and Coauthors, 2007: Will the tropical land biosphere dominate the climate–carbon cycle feedback during the twenty-first century? *Climate Dyn.,* **29,** 565–574, doi:10.1007/s00382-007-0247-8.

Reich, P. B., and S. E. Hobbie, 2013: Decade-long soil nitrogen constraint on the CO_2 fertilization of plant biomass. *Nat. Climate Change,* **3,** 278–282, doi:10.1038/nclimate1694.

Reick, C., T. Raddatz, V. Brovkin, and V. Gayler, 2013: Representation of natural and anthropogenic land cover change in MPI-ESM. *J. Adv. Model. Earth Syst.,* **5,** 459–482, doi:10.1002/jame.20022.

Rodríguez-Fonseca, B., and Coauthors, 2011: Interannual and decadal SST-forced responses of the West African monsoon. *Atmos. Sci. Lett.,* **12,** 67–74, doi:10.1002/asl.308.

Roeckner, E., and Coauthors, 2003: The atmospheric general circulation model ECHAM5. Part I: Model description. Max Planck Institute Tech. Rep. 349, 140 pp. [Available online at http://www.mpimet.mpg.de/fileadmin/publikationen/Reports/max_scirep_349.pdf.]

Roehrig, R., D. Bouniol, F. Guichard, F. Hourdin, and J.-L. Redelsperger, 2013: The present and future of the West African monsoon: A process-oriented assessment of CMIP5 simulations along the AMMA transect. *J. Climate,* **26,** 6471–6505, doi:10.1175/JCLI-D-12-00505.1.

Rowell, D. P., 2012: Sources of uncertainty in future changes in local precipitation. *Climate Dyn.,* **39,** 1929–1950, doi:10.1007/s00382-011-1210-2.

Ruti, P. M., and Coauthors, 2011: The West African climate system: A review of the AMMA model inter-comparison initiatives. *Atmos. Sci. Lett.,* **12,** 116–122, doi:10.1002/asl.305.

Sato, H., A. Itoh, and T. Kohyama, 2007: SEIB–DGVM: A new Dynamic Global Vegetation Model using a spatially explicit individual-based approach. *Ecol. Modell.,* **200,** 279–307, doi:10.1016/j.ecolmodel.2006.09.006.

Scheffran, J., M. Brzoska, J. Kominek, P. M. Link, and J. Schilling, 2012: Climate change and violent conflict. *Science,* **336,** 869–871, doi:10.1126/science.1221339.

Sellers, P. J., and Coauthors, 1996: Comparison of radiative and physiological effects of doubled atmospheric CO_2 on climate. *Science,* **271,** 1402–1406, doi:10.1126/science.271.5254.1402.

Skinner, C. B., M. Ashfaq, and N. S. Diffenbaugh, 2012: Influence of twenty-first-century atmospheric and sea surface temperature forcing on West African climate. *J. Climate,* **25,** 527–542, doi:10.1175/2011JCLI4183.1.

Stein, U., and P. Alpert, 1993: Factor separation in numerical simulations. *J. Atmos. Sci.,* **50,** 2107–2115, doi:10.1175/1520-0469(1993)050<2107:FSINS>2.0.CO;2.

Stevens, B., and Coauthors, 2013: Atmospheric component of the MPI-M Earth System Model: ECHAM6. *J. Adv. Model. Earth Syst.,* **5,** 146–172, doi:10.1002/jame.20015.

Taylor, K. E., R. J. Stouffer, and G. A. Meehl, 2012: An overview of CMIP5 and the experiment design. *Bull. Amer. Meteor. Soc.,* **93,** 485–498, doi:10.1175/BAMS-D-11-00094.1.

Vamborg, F. S. E., V. Brovkin, and M. Claussen, 2011: The effect of a dynamic background albedo scheme on Sahel/Sahara precipitation during the mid-Holocene. *Climate Past,* **7,** 117–131, doi:10.5194/cp-7-117-2011.

Watanabe, S., and Coauthors, 2011: MIROC-ESM 2010: Model description and basic results of CMIP5-20c3m experiments. *Geosci. Model Dev.,* **4,** 845–872, doi:10.5194/gmd-4-845-2011.

Zeng, N., J. D. Neelin, K.-M. Lau, and C. J. Tucker, 1999: Enhancement of interdecadal climate variability in the Sahel by vegetation interaction. *Science,* **286,** 1537–1540, doi:10.1126/science.286.5444.1537.